Please cite this article in press as: Zhu et al., A tridomain model for potassium clearance in optic nerve of *Necturus*, Biophysical Journal (2021), https://doi.org/10.1016/j.bpj.2021.06.020

Biophysical *Journal*
Article

Biophysical Society

A tridomain model for potassium clearance in optic nerve of *Necturus*

Yi Zhu,[1] Shixin Xu,[2,*] Robert S. Eisenberg,[3,4] and Huaxiong Huang[1,5,6]

[1]Department of Mathematics and Statistics, York University, Toronto, Ontario, Canada; [2]Zu Chongzhi Center for Mathematics and Computational Sciences, Division of Natural and Applied Sciences, Duke Kunshan University, Kunshan, China; [3]Department of Applied Mathematics, Illinois Institute of Technology, Chicago, Illinois; [4]Department of Physiology & Biophysics, Rush University, Chicago, Illinois; [5]Research Centre for Mathematics, Advanced Institute of Natural Sciences, Beijing Normal University (Zhuhai), Zhuhai, China; and [6]Division of Science and Technology, BNU-HKBU United International College, Zhuhai, China

ABSTRACT Complex fluids flow in complex ways in complex structures. Transport of water and various organic and inorganic molecules in the central nervous system are important in a wide range of biological and medical processes. However, the exact driving mechanisms are often not known. In this work, we investigate flows induced by action potentials in an optic nerve as a prototype of the central nervous system. Different from traditional fluid dynamics problems, flows in biological tissues such as the central nervous system are coupled with ion transport. They are driven by osmosis created by concentration gradient of ionic solutions, which in turn influence the transport of ions. Our mathematical model is based on the known structural and biophysical properties of the experimental system used by the Harvard group Orkand et al. Asymptotic analysis and numerical computation show the significant role of water in convective ion transport. The full model (including water) and the electrodiffusion model (excluding water) are compared in detail to reveal an interesting interplay between water and ion transport. In the full model, convection due to water flow dominates inside the glial domain. This water flow in the glia contributes significantly to the spatial buffering of potassium in the extracellular space. Convection in the extracellular domain does not contribute significantly to spatial buffering. Electrodiffusion is the dominant mechanism for flows confined to the extracellular domain.

SIGNIFICANCE The central nervous system ("brain") accumulates waste in tiny spaces between cells as thousands of signals move in billions of nerve cells every second. Potassium is dangerous waste because it can paralyze nerves and even kill them. Potassium moves as fluid flows and as it diffuses and migrates in electric fields. We describe glia, nerve cells, and extracellular space of optic nerves by unavoidable partial differential equations and show that potassium poisoning is prevented (mostly) by fluid flow through glia. We suggest that other wastes in the brain are removed by fluid flow through glia as part of the glymphatic system. Mathematics shows how glia pathways help "cleanse the brain" so it can keep on working for many years.

INTRODUCTION

The now-classical experiments of Hodgkin, Huxley, and Katz (1,2) were designed to avoid the artifact of concentration polarization, the (significant) change of concentration of ions as the currents maintaining their voltage clamp flowed across electrodes inside the axon and its membranes. Change of concentration of potassium was seen nonetheless after a few milliseconds of outward potassium currents (3,4), but the change was slow enough to be ignored in their calculations of the action potential (5).

The Kuffler group at Harvard was interested in the role of glia (6,7) in the central nervous system and showed that the membrane potential of the optic nerve of *Necturus* reported the potassium concentration in the narrow extracellular space just outside axons, between glia and axon. Orkand et al. (8) used this membrane potential of glia to report the change in potassium concentration—the polarization of concentration in the narrow extracellular space—as it accumulated during a train of nerve action potentials. Earlier work (3,4) had inferred this concentration change. Orkand et al. (7) measured it quite directly. The artifact of concentration polarization that so worried Hodgkin and Huxley became the experimental reality of potassium accumulation (3) in the central nervous system (8) that interested the Kuffler group.

Submitted December 11, 2020, and accepted for publication June 14, 2021.

*Correspondence: shixin.xu@dukekunshan.edu.cn or hhuang@uic.edu.cn

Editor: Brian Salzberg.

https://doi.org/10.1016/j.bpj.2021.06.020

© 2021 Biophysical Society.

Please cite this article in press as: Zhu et al., A tridomain model for potassium clearance in optic nerve of *Necturus*, Biophysical Journal (2021), https://doi.org/10.1016/j.bpj.2021.06.020

Interest has only grown in the following 50-some odd years.

Potassium accumulation and flow in the extracellular space have been shown to have important roles in many studies focused on aging, Alzheimer's disease, anesthesia, dementia, diabetes, epilepsy, migraine, sleep, stroke, and traumatic brain injury. Potassium accumulation and flow play an important role in the biology of the central nervous system (9), normal and abnormal (10–16). The glymphatic model has received much interest in the last months. It links potassium accumulation, flows in the extracellular space—particularly in sleep and diseases of aging—with general disposal of waste through glial pathways to the circulatory system (9,17–21).

The accumulation of ions in a narrow extracellular space, such as that between nerve and glia or Schwann cell (4), depends on the diffusion, convection, and migration of ions in an electric field. Convection is likely to be important. Evolution uses the circulatory system to provide convective transport close to nearly every cell in a mammal, the lens of the eye being a notable exception, so the delays involved in electrodiffusion are overcome. Convection provides what diffusion denies: speed.

The optic nerve, and the mammalian central nervous system in general, involves nerve, glia, and narrow extracellular space. It involves three types of flow—convection, diffusion, and migration—in the electric field in radial and longitudinal directions of a cylindrical structure. It involves (chiefly) three ions (K, Na, and Cl), and a number of different types of channels and pumps (voltage-activated Na channels and at least two types of K channels and the Na/K pump). The description and analysis, not to mention the numerical computation of the optic nerve, must deal with what is actually in the optic nerve. It must deal with what evolution has actually built in the central nervous system in general. Thus, the analysis must involve many forces, flows, structures, and channels and transporters. Here, we report the subset of our work that deals with the accumulation of potassium in the narrow extracellular space of optic nerve.

The interactions between neuronal cells and glial cells have been included in models of the important phenomenon of spreading depression (22–25) thought to be related to epilepsy and migraine. Some two-compartment models for potassium clearance (or spatial buffering) include interactions between neuron cells and extracellular space (26) or interactions between glial cells and extracellular space (27–29). A tricompartment model using ordinary differential equations was introduced by Sibille (30) to study the role of K_{ir4} channels. It shows that the flows play an important role in the central nerve system (31) via influx and efflux routes to help waste clearance, which has been called (with understandable enthusiasm, if not hyperbole) a final frontier of neuroscience (32). Some models, including flow but not electrodiffusion, were introduced to study the pressure effect on the flow (33–36). Mori (15) proposed a multidomain model for cortical spreading depression, in which ionic electrodiffusion and osmosis between different compartments are considered. In this work, we first extend those results and the two-compartment structural analysis of the spherical lens (37) to the three-compartment cylindrical optic nerve fiber of *Necturus*. Then, we present some general conclusions based on the analysis of a specific set of experiments by Orkand et al. (7,8) using a model distributed in space in both radial and longitudinal directions and that involves action potentials generated by Hodgkin-Huxley equations.

This work is organized as follows. The full model for microcirculation of water and ions are proposed based on conservation laws in Mathematical model. Then, the model is calibrated and aligned with the Orkand experiment results in Model calibration. In Potassium clearance, the calibrated model is used to study the flow and ion microcirculations during Potassium clearance. A discussion on the parameters is presented in Results and discussion. Then, the conclusions and future work are given in Conclusions.

MATERIALS AND METHODS

Mathematical model

In this section, we present a tridomain model for microcirculation of the optic nerve. The model deals with two types of flow: the circulation of water (hydrodynamics) and the circulation of ions (electrodynamics) in the glial compartment (Ω_{gl}), axon compartment (Ω_{ax}), and extracellular space (Ω_{ex}).

The glial compartment and axon compartment exist only in the optic nerve, whereas extracellular space exists both in the optic nerve Ω_{ex}^{OP} and subarachnoid space Ω_{ex}^{SAS} (see Fig. 1):

$$\Omega_{OP} = \Omega_{ax} \cup \Omega_{gl} \cup \Omega_{ex}^{OP}, \quad \Omega_{SAS} = \Omega_{ex}^{SAS}.$$

The model is mainly derived from laws of conservation of ions and water for flow through membranes between intracellular compartments and extracellular space (38).

Notations and assumptions

We first introduce the following notations used in the study, in which $i = Na^+$, K^+, or Cl^- for ion species; $l = ex$, gl, and ax for extracellular space, glial compartment, and axon compartment; and $k = gl$ or ax for glial or axon membrane in the optic nerve.

Fig. 1 *b* shows the model with the whole domain Ω that consists of the subarachnoid space (SAS) region Ω_{SAS} and optic nerve region Ω_{OP} (see Fig. 2),

$$\Omega = \Omega_{SAS} \cup \Omega_{OP}.$$

In the optic nerve region Ω_{OP}, the glial membrane and axon membrane separate domains Ω_{gl} and Ω_{ax} from the extracellular region Ω_{ex}^{OP}, respectively (also see Fig. 1). Based on the structure of the optic nerve, we have the following global assumptions for the model.

Charge neutrality. In each domain, we assume that there is electroneutrality

$$\eta_{gl} \sum_i z^i C_{gl}^i + z^{gl} \eta_{gl}^{re} A_{gl} = 0, \tag{1a}$$

Please cite this article in press as: Zhu et al., A tridomain model for potassium clearance in optic nerve of *Necturus*, Biophysical Journal (2021), https://doi.org/10.1016/j.bpj.2021.06.020

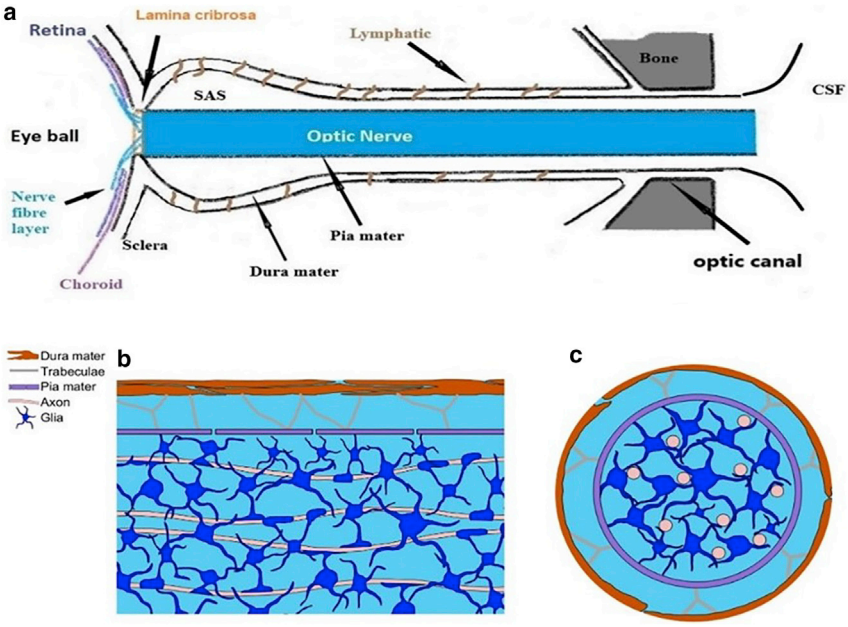

FIGURE 1 Optic nerve structure. (*a*) Key features of the optic nerve region and subarachnoid space (SAS); (*b*) longitudinal section of the optic nerve; (*c*) cross section of the optic nerve. To see this figure in color, go online.

$$\eta_{ax}\sum_i z^i C^i_{ax} + z^{ax}\eta^{re}_{ax}A_{ax} = 0, \tag{1b}$$

and

$$\sum_i z^i C^i_{ex} = 0, \tag{1c}$$

where $A_l > 0$ with $l = ax$ or gl is the density of proteins in axons or glial cells. The proteins are negatively charged, but the charge density is customarily described by a positive number. The η_{ax} and η_{gl} are the volume fraction of axon and glial compartments in the optic nerve, and η^{re}_{ax} and η^{re}_{gl} are the resting state volume fractions.

Axial symmetry. For simplicity, axial symmetry is assumed. The model can be straightforwardly extended to three dimensions when data and needs justify the considerable extra computational resources needed to analyze such models.

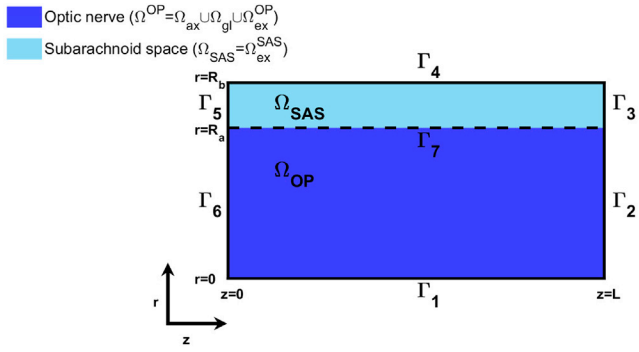

FIGURE 2 Domain of the axial symmetry model. The optic nerve Ω_{OP} consist of axon compartment Ω_{ax}, glial compartment Ω_{gl}, and extracellular space Ω^{OP}_{ex}. The subarachnoid space only has extracellular space Ω^{SAS}_{ex}. $R_a = 48\ \mu$m is the radius of optic nerve, and $R_b = 60\ \mu$m is the radius from optical nerve center to the dura mater. To see this figure in color, go online.

Isotropy of glial compartment and extracellular space.

1) The extracellular space forms a narrow structure of branching clefts surrounding the glial cells and nerve axons.
2) The glial cells are connected to each other by connexins and form a syncytium.
3) The extracellular space is continuous and forms a syncytium.

Both syncytia are assumed isotropic here, until we know better. The axons are not connected to each other. For $l = gl$ and ex and $i = Na^+$, K^+, or Cl^-, the ion flux and water flow velocity are in the following forms:

$$\boldsymbol{j}^i_l = j^i_{l,r}\widehat{\boldsymbol{r}} + j^i_{l,z}\widehat{\boldsymbol{z}} \tag{2}$$

and

$$\boldsymbol{u}_l = u^r_l\widehat{\boldsymbol{r}} + u^z_l\widehat{\boldsymbol{z}}. \tag{3}$$

Anisotropy of axon compartment. The axons are separated, more or less parallel cylindrical cells that do not form a syncytium. For $i = Na^+$, K^+, or Cl^-, the ion flux and water flow velocity are in the following forms:

$$\boldsymbol{j}^i_{ax} = j^i_{ax,z}\widehat{\boldsymbol{z}} \tag{4}$$

and

$$\boldsymbol{u}_{ax} = u^z_{ax}\widehat{\boldsymbol{z}}. \tag{5}$$

Communications between compartments. The communications between intracellular compartments and extracellular space are through membranes. There is no direct interaction between glial and axon compartments. Interactions occur only through changes in concentration, electrical potential, and flows in the extracellular space (30).

The interface of optic nerve and SAS is the pia mater denoted by Γ_7,

$$\Omega_{OP} \cap \Omega_{SAS} = \Gamma_7.$$

Please cite this article in press as: Zhu et al., A tridomain model for potassium clearance in optic nerve of *Necturus*, Biophysical Journal (2021), https://doi.org/10.1016/j.bpj.2021.06.020

In our model, both pia mater Γ_7 and dura mater Γ_4 are modeled as macroscopic membranes and appropriate boundary conditions. The transmembrane water flow through pia mater (39) depends on hydrostatic pressure, osmotic pressure, and electric potential, whereas that through dura mater only depends on the hydrostatic pressure.

For the domain boundaries, Γ_1 is the radius center of the optic nerve; Γ_2 and Γ_3 are the far end (away from the eyeball) of the optic nerve that is connected to the optic canal region (40). Γ_5 is used to model the dura mater connected to the sclera (the white matter of the eye) and assumed to be nonpermeable (41). Γ_6 is used to denote the lamina cribrosa, where the optic nerve head exits the eye posteriorly through pores of the lamina cribrosa (42).

Water circulation

We model water circulation with the following assumptions:

- the loss or gain of water in axons and glial cells is only through membranes flowing into or out of the extracellular space,
- the transmembrane water flux is proportional to the intra- or extracellular hydrostatic pressure and osmotic pressure differences, and
- the glial cell and axons can swell and shrink because of the water inflows and outflows.

We use $\eta_l(r, z, t)$ to describe the volume fraction of the l region ($l = gl, ax,$ and ex), which varies over time and space because of transmembrane water flows. The conservation of water in each domain yields

$$\frac{\partial \eta_{gl}}{\partial t} + \mathcal{M}_{gl} U^m_{gl} + \nabla \cdot \left(\eta_{gl} \boldsymbol{u}_{gl}\right) = 0, \tag{6a}$$

$$\frac{\partial \eta_{ax}}{\partial t} + \mathcal{M}_{ax} U^m_{ax} + \frac{\partial}{\partial z}\left(\eta_{ax} u^z_{ax}\right) = 0, \tag{6b}$$

and

$$\nabla \cdot \left(\eta_{gl} \boldsymbol{u}_{gl}\right) + \nabla \cdot \left(\eta_{ex} \boldsymbol{u}_{ex}\right) + \frac{\partial}{\partial z}\left(\eta_{ax} u^z_{ax}\right) = 0, \tag{6c}$$

where we use the fact that density of water is constant. Here, $\boldsymbol{u}_l$ with $l = gl$, ax, and ex is the velocity in the glial cells, axons, and extracellular space, respectively. The transmembrane water flow U^m_k with $k = gl$ or ax follows Starling's law on the kth membrane,

$$U^m_{gl} = L^m_{gl}\left(P_{gl} - P_{ex} - \gamma_{gl} k_B T \left(O_{gl} - O_{ex}\right)\right)$$

and

$$U^m_{ax} = L^m_{ax}\left(P_{ax} - P_{ex} - \gamma_{ax} k_B T \left(O_{ax} - O_{ex}\right)\right).$$

The P_l with $l = gl$, ax, and ex are the hydrostatic pressure in the glial cells, axons, and extracellular space, respectively, and $k_B T O_l$ is the osmotic pressure (37,43) defined by

$$O_{ex} = \sum_i C^i_{ex}, \quad O_l = \sum_i C^i_l + A_l \frac{\eta^{re}_j}{\eta_l}, \quad l = gl, ax,$$

where $A_l \frac{\eta^{re}_l}{\eta_l} > 0$ is the density of the permanent negatively charged protein in glial cells and axons that varies with the volume (fraction) of the region. In this work, we assume the permanent negatively charged protein is uniformly distributed within glial cells and axons and has valence z^l, $l = gl$ or ax. The $\mathcal{M}_k$ and γ_k, $k = gl$ or ax are the glial cells (or axons) membrane area per unit volume and membrane reflection coefficient (44), respectively. L^m_{gl} and L^m_{ax} are the surface membrane hydraulic permeabilities of glial cells and axons. The membrane reflection coefficient γ_k ($k = gl$ or ax) is the ratio between the observed osmotic pressure and theoretical osmotic pressure. k_B is the Boltzmann constant, and T is temperature.

For the volume fraction η_l, $l = gl$, ax, or ex, we have

$$\eta_{gl} + \eta_{ax} + \eta_{ex} = 1, \quad \text{in } \Omega. \tag{7}$$

Note the glial cells and axons are found only in the Ω_{OP} region. In other words, $\eta_{ax} = \eta_{gl} \equiv 0$ and $\eta_{ex} \equiv 1$ are fixed in Ω_{SAS}. Therefore, the solution is incompressible in Ω_{SAS}, and we have

$$\nabla \cdot \boldsymbol{u}_{ex} = 0, \text{ in } \Omega_{SAS}. \tag{8}$$

The relation between the hydrostatic pressure P_l and volume fraction η_l ($l = gl$, ax, or ex) is connected by the force balance on the membrane $\mathcal{M}_k$ ($k = gl$ or ax). The membrane force is balanced with the hydrostatic pressure difference on both sides of the semipermeable membrane (15,43). Then, the variation of volume fraction from the resting state is proportional to the variation of hydrostatic pressure difference from the resting state:

$$K_{gl}\left(\eta_{gl} - \eta^{re}_{gl}\right) = P_{gl} - P_{ex} - \left(P^{re}_{gl} - P^{re}_{ex}\right) \tag{9a}$$

or

$$K_{ax}\left(\eta_{ax} - \eta^{re}_{ax}\right) = P_{ax} - P_{ex} - \left(P^{re}_{ax} - P^{re}_{ex}\right), \tag{9b}$$

where $K_{gl,ax}$ is the stiffness constant and η^{re}_l and P^{re}_l ($l = gl$, ax, or ex) are the resting state volume fraction and hydrostatic pressure.

The osmotic pressure influences the volume fraction in an implicit way. Because of Eq. 6 and the definition of transmembrane water flow U^m_{gl}, the osmotic pressure difference induces the transmembrane water flow going in and out of compartments, and the hydrostatic pressure changes correspondingly.

In reality, both dura mater Γ_7 and pia mater Γ_4 are deformable. However, the stiffnesses of them are much larger than glial cells' (45–47). For the sake of simplicity, we neglect the deformation of dura mater and pia mater so the system could be solved in fixed domains Ω and Ω^{OP}. We are aware that in some important clinical applications, the deformation is of great importance and that our model will need to be extended to deal with them. The extensions do not produce analytical challenges, but they are likely to add significant complexity to the numerical methods and make the computations much more involved and longer.

Note that the concentrations of ions and effective concentration of water vary a great deal and so are described by equations in which the number density of ions and effective number density of water vary in both the radial and longitudinal directions according to conservation laws, without using compartments that may not have unique definitions or relations to anatomical structures. Indeed, the variation of concentration is one of the main determinants of the properties of ionic solutions. The solution is incompressible, the components are not (48).

Next, we define the velocity in each domain.

Water velocities in the glial compartment. As we mentioned before, the glial cells are connected through the narrow connections on the membranes and form a syncytium. The fluid velocity inside the compartment is limited by the transmembrane fluid velocity, which is determined by the difference of hydro pressure and osmotic pressure on both sides of the membrane (15,43). On the macro scale, by using averaging process (37,49,50), the glial compartment is treated with membranes everywhere. So, the velocity of fluid in glial syncytium $\boldsymbol{u}_{gl}$ depends on the gradients of hydrostatic pressure and osmotic pressure:

$$u^r_{gl} = -\frac{\kappa_{gl} \tau_{gl}}{\mu}\left(\frac{\partial P_{gl}}{\partial r} - \gamma_{gl} k_B T \frac{\partial O_{gl}}{\partial r}\right) \tag{10a}$$

and

Please cite this article in press as: Zhu et al., A tridomain model for potassium clearance in optic nerve of *Necturus*, Biophysical Journal (2021), https://doi.org/10.1016/j.bpj.2021.06.020

$$u_{gl}^{z} = -\frac{\kappa_{gl}\tau_{gl}}{\mu}\left(\frac{\partial P_{gl}}{\partial z} - \gamma_{gl}k_B T\frac{\partial O_{gl}}{\partial z}\right). \tag{10b}$$

Substituting Eq. 10a into the incompressibility (Eq. 6a) yields a Poisson equation for pressure in the glial compartment. The boundary conditions in the glial syncytium are as follows:

$$\begin{cases} \dfrac{\partial P_{gl}}{\partial r} = 0, & \text{on } \Gamma_1 \cup \Gamma_7, \\ \dfrac{\partial P_{gl}}{\partial z} = 0, & \text{on } \Gamma_2 \cup \Gamma_6, \end{cases} \tag{11}$$

where a homogeneous Neumann boundary condition is applied at all four of these boundaries.

Water velocity in the axon compartment. Axons are arranged parallel in the longitudinal direction and are isolated from each other. The fluid velocity in the axon compartment is defined along z direction as

$$u_{ax}^{r} = 0 \tag{12a}$$

and

$$u_{ax}^{z} = -\frac{\kappa_{ax}}{\mu}\frac{\partial P_{ax}}{\partial z}. \tag{12b}$$

Similarly, substituting the above velocity into the incompressibility equation gives the Poisson equation for pressure in the axon compartment. A homogeneous Neumann condition for pressure is used on the left and right boundaries of the axon compartment:

$$\frac{\partial P_{ax}}{\partial z} = 0, \text{ on } \Gamma_2 \cup \Gamma_6. \tag{13}$$

Velocity in the extracellular space. The extracellular space is a narrow connected domain, where the electro-osmotic effect needs to be considered (37,51,52). The extracellular velocity is determined by the gradients of hydrostatic pressure and electric field

$$u_{ex}^{r} = -\frac{\kappa_{ex}\tau_{ex}}{\mu}\frac{\partial P_{ex}}{\partial r} - k_e\tau_{ex}\frac{\partial \phi_{ex}}{\partial r} \tag{14a}$$

and

$$u_{ex}^{z} = -\frac{\kappa_{ex}\tau_{ex}}{\mu}\frac{\partial P_{ex}}{\partial z} - k_e\tau_{ex}\frac{\partial \phi_{ex}}{\partial z}, \tag{14b}$$

where ϕ_{ex} is the electric potential in the extracellular space, τ_{ex} is the tortuosity of extracellular region (38,53), μ is the viscosity of water, k_e describes the effect of electro-osmotic flow (51,52,54), and κ_{ex} is the permeability of the extracellular space. Here, the hydro permeability κ_{ex}, tortuosity τ_{ex}, and electric-osmotic parameter k_e have two distinguished values in the region Ω_{ex}^{OP} and Ω_{ex}^{SAS},

$$\kappa_{ex} = \begin{cases} \kappa_{ex}^{OP}, & \text{in } \Omega_{OP}, \\ \kappa_{ex}^{SAS}, & \text{in } \Omega_{SAS}, \end{cases} \quad \tau_{ex} = \begin{cases} \tau_{ex}^{OP}, & \text{in } \Omega_{OP}, \\ \tau_{ex}^{SAS}, & \text{in } \Omega_{SAS}, \end{cases} \tag{15}$$

$$k_e = \begin{cases} k_e^{OP}, & \text{in } \Omega_{OP}, \\ k_e^{SAS}, & \text{in } \Omega_{SAS}. \end{cases}$$

By substituting the definitions of velocities Eqs. 10a, 12a, and 14a and volume fractions Eq. 9a into the mass conservation law Eq. 6, it yields the evolution equations of hydrostatic pressure in different compartments, which are solved during the simulations in session 4.

Because $\Gamma_2 \cup \Gamma_3$ are the far end of the optic nerve away from the eyeball and connect to the optic canal, we assume the hydrostatic pressure of extracellular fluid is equal to the cerebrospinal fluid pressure. On the other hand, the intraocular pressure (IOP) is imposed at Γ_6, where the extracellular space is connected to the retina. At the boundary Γ_5, we assume a nonpermeable boundary. We are aware of the significance of the pressures and flows at these boundaries for clinical phenomena, including glaucoma (36,55,56), and will return to that subject in later publications.

The water flow across the semipermeable membrane Γ_4 is produced by the lymphatic drainage on the dura membrane, which depends on the difference between extracellular pressure and orbital pressure (OBP). We assume the velocity across the pia membrane Γ_4, is continuous and determined by the hydrostatic pressure and osmotic pressure. To summarize, the boundary conditions of the extracellular fluid are

$$\begin{cases} \boldsymbol{u}_{ex}\cdot\hat{\boldsymbol{r}} = 0, & \text{on } \Gamma_1, \\ P_{ex} = P_{CSF}, & \text{on } \Gamma_2 \cup \Gamma_3, \\ \boldsymbol{u}_{ex}^{SAS}\cdot\hat{\boldsymbol{r}} = L_{dr}^{m}\left(P_{ex}^{SAS} - P_{OBP}\right), & \text{on } \Gamma_4, \\ \boldsymbol{u}_{ex}\cdot\hat{\boldsymbol{z}} = 0, & \text{on } \Gamma_5, \\ P_{ex} = P_{IOP}, & \text{on } \Gamma_6, \\ \boldsymbol{u}_{ex}^{OP}\cdot\hat{\boldsymbol{r}} = \boldsymbol{u}_{ex}^{SAS}\cdot\hat{\boldsymbol{r}} \\ \quad = L_{pia}^{m}\left(P_{ex}^{OP} - P_{ex}^{SAS} - \gamma_{pia}k_B T\left(O_{ex}^{OP} - O_{ex}^{SAS}\right)\right), & \text{on } \Gamma_7, \end{cases} \tag{16}$$

where P_{CSF} is the cerebrospinal fluid pressure (36), P_{IOP} is the intraocular pressure, and P_{OBP} is the orbital pressure on the dura mater.

Ion transport

For ion circulation, we assume

- only three types of ions are considered: Na^+, K^+, and Cl^-;
- the sodium-potassium ATP pump is present on both glial and axon membranes;
- ion channel conductance on glial cell membranes is a fixed constant, independent of the voltage and time. The sodium conductance is assumed small, and its channel origin unknown. The potassium conductance is large and comes from the K_{ir4} channels (31,57). When experimental evidence is available, other types of pumps and channels can be added to the model; and
- sodium channel and potassium channel conductance on axons are voltage gated, whereas the conductance of chloride channel is fixed.

The conservation of ions implies the following system of partial differential equations to describe the dynamics of ions in each region, for $i = Na^+$, K^+, or Cl^-:

$$\frac{\partial\left(\eta_{gl}C_{gl}^{i}\right)}{\partial t} + \mathcal{M}_{gl}J_{gl}^{m,i} + \nabla\cdot\left(\eta_{g}\boldsymbol{j}_{gl}^{i}\right) = 0, \tag{17a}$$

$$\frac{\partial\left(\eta_{ax}C_{ax}^{i}\right)}{\partial t} + \mathcal{M}_{ax}J_{ax}^{m,i} + \frac{\partial}{\partial z}\left(\eta_{ax}j_{ax,z}^{i}\right) = 0, \tag{17b}$$

Please cite this article in press as: Zhu et al., A tridomain model for potassium clearance in optic nerve of *Necturus*, Biophysical Journal (2021), https://doi.org/10.1016/j.bpj.2021.06.020

and

$$\frac{\partial\left(\eta_{ex}C^i_{ex}\right)}{\partial t}-\mathcal{M}_{ax}J^{m,i}_{ax}-\mathcal{M}_{gl}J^{m,i}_{gl}+\nabla\cdot\left(\eta_{ex}\boldsymbol{j}^i_{ex}\right)=0, \quad (17c)$$

where the last equation reduces to the following in the Ω_{SAS} region,

$$\frac{\partial C^{i,SAS}_{ex}}{\partial t}+\nabla\cdot\boldsymbol{j}^{i,SAS}_{ex}=0. \quad (18)$$

The transmembrane ion flux $J^{m,i}_k$ ($k = gl$ or ax) consists of active ion pump source a^i_k and passive ion channel source b^i_k for ion i on the axon ($k = ax$) or glial cell membranes ($k = gl$). In the glial cell membranes,

$$J^{m,i}_k=a^i_k+b^i_k, \quad k=gl,ax, \quad i=\mathrm{Na}^+,\mathrm{K}^+,\mathrm{Cl}^-.$$

In the glial cell membranes, b^i_{gl} is defined as

$$b^i_{gl}=\frac{g^i_{gl}}{z^ie}\left(\phi_{gl}-\phi_{ex}-E^i_{gl}\right), \quad (19)$$

where the Nernst potential is used to describe the gradient of chemical potential $E^i_{gl}=\frac{k_BT}{ez^i}\log\left(\frac{C^i_{ex}}{C^i_{gl}}\right)$ and the conductance g^i_{gl} for each ion on the glial membrane is a fixed constant, independent of voltage and time. On the axon's membrane, b^i_{ax} is defined as

$$b^i_{ax}=\frac{g^i_{ax}}{z^ie}\left(\phi_{ax}-\phi_{ex}-E^i_{ax}\right), \quad (20)$$

where

$$g^{Na}_{ax}=\overline{g}^{Na}m^3h+g^{Na}_{leak}, \quad g^K_{ax}=\overline{g}^Kn^4+g^K_{leak},$$

$$E^i_{ax}=\frac{k_BT}{ez^i}\log\left(\frac{C^i_{ex}}{C^i_{ax}}\right).$$

The time-dependent dynamic of open probability, often loosely called "gating," is governed by the Hodgkin-Huxley model (58,59)

$$\frac{dn}{dt}=\alpha_n(1-n)-\beta_nn, \quad (21a)$$

$$\frac{dm}{dt}=\alpha_m(1-m)-\beta_mm, \quad (21b)$$

and

$$\frac{dh}{dt}=\alpha_h(1-h)-\beta_hh. \quad (21c)$$

We assume that the only pump is the Na/K active transporter. We are more than aware that other active transport systems can and likely do move ions and water in this system. They will be included as experimental information becomes available.

In the case of the Na/K pump a^i_l, $l = ax$ or gl, the strength of the pump depends on the concentration in the intracellular and extracellular space (59,60), i.e.,

$$a^{Na}_k=\frac{3I_k}{e}, \ a^K_k=-\frac{2I_k}{e}, \ a^{Cl}_k=0, \ k=gl,ax, \quad (22)$$

where

$$I_k=I_{k,1}\left(\frac{c^{Na}_k}{c^{Na}_k+K_{Na1}}\right)^3\left(\frac{c^K_{ex}}{c^K_{ex}+K_{K1}}\right)^2$$

$$+I_{k,2}\left(\frac{c^{Na}_k}{c^{Na}_k+K_{Na2}}\right)^3\left(\frac{c^K_{ex}}{c^K_{ex}+K_{K2}}\right)^2.$$

$I_{k,1}$ and $I_{k,2}$ are related to the α_1- and α_2-isoforms of the Na/K pump.

The definitions of ion flux in each domain are as follows, for $i = \mathrm{Na}^+$, K^+, and Cl^-:

$$\boldsymbol{j}^i_l=C^i_l\boldsymbol{u}_l-D^i_l\tau_l\left(\nabla C^i_l+\frac{z^ie}{k_BT}C^i_l\nabla\phi_l\right), \ l=gl,ex \quad (23a)$$

and

$$j^i_{ax,z}=C^i_{ax}u^z_{ax}-D^i_{ax}\left(\frac{\partial C^i_{ax}}{\partial z}+\frac{z^ie}{k_BT}C^i_{ax}\frac{\partial\phi_{ax}}{\partial z}\right). \quad (23b)$$

For the axon compartment boundary condition, we have

$$C^i_{ax}=C^{i,re}_{ax} \quad \text{on} \ \ \Gamma_2\cup\Gamma_6$$

and

$$\begin{cases}\dfrac{\partial C^i_{gl}}{\partial r}=0 & \text{on } \Gamma_1,\\ C^i_{gl}=C^{i,re}_{gl} & \text{on } \Gamma_2\cup\Gamma_6,\\ \boldsymbol{j}^i_{gl}\cdot\hat{\boldsymbol{r}}=0 & \text{on } \Gamma_7,\end{cases}$$

where the Dirichlet boundary conditions are used at locations $\Gamma_2 \cup \Gamma_6$ for axons and glial cell and a nonflux boundary condition is used for glial cell ion flux on the radius center Γ_1 and pia mater Γ_7 .

For the extracellular space boundary condition, similar boundary conditions are imposed except on the pia mater Γ_7. The flux across the pia mater is assumed continuous, and Ohm's law is used (37). Additionally, a nonpermeable boundary condition is used at location Γ_5, and a homogeneous Neumann boundary condition is applied at the location of the dura mater Γ_4,

$$\begin{cases}\dfrac{\partial C^i_{ex}}{\partial r}=0, & \text{on } \Gamma_1,\\ C^i_{ex}=C^i_{csf}, & \text{on } \Gamma_2\cup\Gamma_3,\\ \dfrac{\partial C^i_{ex}}{\partial r}=0, & \text{on } \Gamma_4,\\ \boldsymbol{j}^i_{ex}\cdot\hat{\boldsymbol{z}}=0, & \text{on } \Gamma_5,\\ C^i_{ex}=C^i_{IOP}, & \text{on } \Gamma_6,\\ \boldsymbol{j}^{i,OP}_{ex}\cdot\hat{\boldsymbol{r}}=\boldsymbol{j}^{i,SAS}_{ex}\cdot\hat{\boldsymbol{r}}=\dfrac{G^i_{pia}}{z^ie}\left(\phi^{OP}_{ex}-\phi^{SAS}_{ex}-E^i_{pia}\right), & \text{on } \Gamma_7.\end{cases} \quad (24)$$

Please cite this article in press as: Zhu et al., A tridomain model for potassium clearance in optic nerve of *Necturus*, Biophysical Journal (2021), https://doi.org/10.1016/j.bpj.2021.06.020

Multiplying equations in Eqs. 17a, 17b, and 17c with $z_i e$, respectively, summing up, and using Eqs. 1a, 1b, and 1c) and Eq. 23, we have the following system for the electric potential in *ax*, *gl*, or *ex*:

$$\sum_i z^i e \mathcal{M}_{gl} J^{m,i}_{gl} + \sum_i \nabla \cdot \left(z^i e \eta_g \boldsymbol{j}^i_{gl} \right) = 0, \tag{25a}$$

$$\sum_i z^i e \mathcal{M}_{ax} J^{m,i}_{ax} + \sum_i \frac{\partial}{\partial z} \left(z^i e \eta_{ax} j^i_{ax,z} \right) = 0, \tag{25b}$$

and

$$\sum_i \nabla \cdot \left(z^i e \eta_{gl} \boldsymbol{j}^i_{gl} \right) + \sum_i \frac{\partial}{\partial z} \left(z^i e \eta_{ax} j^i_{ax,z} \right) + \sum_i \nabla \cdot \left(z^i e \eta_{ex} \boldsymbol{j}^i_{ex} \right) = 0, \tag{25c}$$

which describe the spatial distributions of electric potentials in three compartments.

In the subarachnoid space Ω_{SAS}, the governing equation for extracellular electric potential reduces to

$$\nabla \cdot \left(\sum_i z^i e \boldsymbol{j}^{i,SAS}_{ex} \right) = 0. \tag{26}$$

The boundary conditions for electric fields ϕ_{ax}, ϕ_{gl}, and ϕ_{ex} are given below.

In the axon compartment,

$$\begin{cases} \dfrac{\partial \phi_{ax}}{\partial z} = 0, & \text{on } \Gamma_2, \\ \dfrac{\partial \phi_{ax}}{\partial z} = 0, & \text{on } \Gamma_6; \end{cases}$$

in the glial compartment,

$$\begin{cases} \dfrac{\partial \phi_{gl}}{\partial r} = 0, & \text{on } \Gamma_1, \\ \dfrac{\partial \phi_{gl}}{\partial z} = 0, & \text{on } \Gamma_2, \\ \dfrac{\partial \phi_{gl}}{\partial z} = 0, & \text{on } \Gamma_6, \\ \dfrac{\partial \phi_{gl}}{\partial r} = 0, & \text{on } \Gamma_7; \end{cases}$$

and in the extracellular space,

$$\begin{cases} \dfrac{\partial \phi_{ex}}{\partial r} = 0, & \text{on } \Gamma_1, \\ \dfrac{\partial \phi_{ex}}{\partial z} = 0, & \text{on } \Gamma_2 \cup \Gamma_3, \\ \dfrac{\partial \phi_{ex}}{\partial r} = 0, & \text{on } \Gamma_4, \\ \dfrac{\partial \phi_{ex}}{\partial z} = 0, & \text{on } \Gamma_5, \\ \dfrac{\partial \phi_{ex}}{\partial z} = 0, & \text{on } \Gamma_6, \\ \sum_i z^i e \boldsymbol{j}^{i,OP}_{ex} \cdot \hat{\boldsymbol{r}} = \sum_i z^i e \boldsymbol{j}^{i,SAS}_{ex} \cdot \hat{\boldsymbol{r}} & \\ = \sum_i G^i_{pia} \left(\phi^{OP}_{ex} - \phi^{SAS}_{ex} - E^i_{pia} \right), & \text{on } \Gamma_7. \end{cases} \tag{27}$$

Model calibration

Our work is possible because of and was motivated by the study of Orkand et al. (7,8) that measured the accumulation of potassium in the narrow extracellular space (Ω^{OP}_{ex}) of the optic nerve of the amphibian salamander *Necturus*, in the spirit of the original work of Frankenhaeuser and Hodgkin (4), which first identified and analyzed accumulation of potassium outside a nerve fiber. The existence and qualitative properties of that accumulation of potassium were known to and a cause for concern for Hodgkin from his first work on the voltage clamp (1,2), if not earlier. Hodgkin described the phenomena as part of what was called (concentration) "polarization" and discussed it extensively with students sometime later (Eisenberg, personal communication, 1962).

The key experiment in the Orkand study (8) measures the change in potential across the glial membrane produced by a train of action potentials. The glial membrane potential is used to estimate and report the potassium concentration in the narrow extracellular space, because the glial membrane is populated with more or less voltage-independent potassium channels and not much else.

In the experiment, optic nerve has been put in three different K^+ concentrations (1.5, 3, or 4.5 mM) in the bathing solution to change the resting potential across the glia membrane. Then, the axon was stimulated to give a train of action potentials. The action potentials increased K^+ in Ω^{OP}_{ex}. The accumulated K^+ then made the glia membrane potential more positive. Stimuli were applied at both ends of a region of the optic nerve, thereby producing a more uniform (in space) potential within that region.

The model of this system is solved by using the finite volume method with mesh size $h = 1/20$ and temporal size $t = 1/10$ in dimensionless units. The code is written and executed in the MATLAB environment (The MathWorks, Natick, MA). The flowchart for the simulation is shown in Fig. 3. In the first step, we obtain the resting state of the system by iteration and fixed volume fraction (7)

$$\eta^{re}_{ax} = 0.5,\ \eta^{re}_{gl} = 0.4,\ \eta^{re}_{ex} = 0.1.$$

In the dynamic process, the resting state values are taken as initial values. Then, we first solve the concentration governing equations, followed by the electrical potential equation and pressure equations. We update the volume fraction by using Eqs. 9a and 9b.

In our simulation study, we first set the extracellular space (Ω^{OP}_{ex}) concentration of K^+ to be 3 mM and obtained a resting potential across the glial

Please cite this article in press as: Zhu et al., A tridomain model for potassium clearance in optic nerve of *Necturus*, Biophysical Journal (2021), https://doi.org/10.1016/j.bpj.2021.06.020

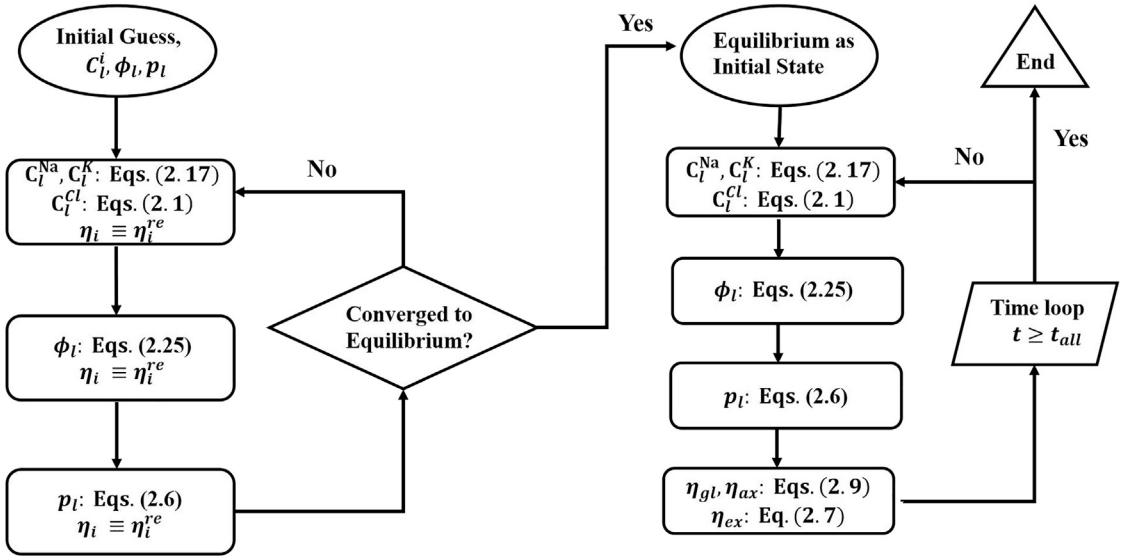

FIGURE 3 Flowchart for simulation process.

membrane (∼−89 mV). In Orkand's work (7,8), suction electrodes were used for stimulating; the two ends of the optic nerve were placed in suction electrodes, as described in their Methods section. We modeled the suction electrodes by applying a train of rectangular function (sometimes called a "box car" stimulus in the engineering literature) currents through the axon membrane at $z = 2.25$ mm, 13.5 mm, and $0 < r < R_a = 48$ μm. Each stimulus in the train lasted 3 ms (as Orkand's work indicated) with current strength 3 mA/m^2. The stimulus was large enough to exceed the threshold and generate action potentials. After a train of stimuli with a frequency of 17/s for 1 s, the first panel of Fig. 4 shows the train of axon membrane action potentials and its return to the initial level (∼−89 mV) after 1 s. The profiles of the first action potential and the last action potential in the train are presented in the second panel. The third and fourth panels are used to illustrate the increase in glial cell membrane potential and extracellular potassium concentration during and after the train of stimuli. The fourth panel of Fig. 4 shows that during stimulus, the K^+ concentration in Ω_{ex}^{OP} keeps increasing because of the opening of the voltage-gated potassium channel of the axon membrane. As a result of the accumulated K^+ in Ω_{ex}^{OP}, the membrane potential of glial cells also continues to increase until the stimulus stops.

Then, we vary the K^+ to be 1.5, 3, 4.5 mM in Ω_{ex}^{OP} and record the magnitude of the maximal glial membrane depolarized potential in each case as in Fig. 5. The black symbols are used for experimental data, and red ones are the simulation results of our model. Fig. 5 shows that our model could match the experimental resting potentials (*solid symbols*) and depolarization potentials (*open symbols*) very well with different K^+ concentrations in Ω_{ex}^{OP}.

Our work is limited by the lack of other types of data for calibration, although it is important to remember that the structural parameters, values of membrane capacitance, many conductance variables, and resistivities of bulk solutions are known quite well because of the work of generations of anatomists, physiologists, and biophysicists.

Potassium clearance

In this section, we compare the potassium clearance under various conditions based on the full model. In Alternative distribution of stimulus location, by applying the stimuli at alternative locations on the axon, we show how the interaction between the extracellular pathway and glial transmembrane pathway helps potassium clearance. The microcirculation patterns of water and ions between glial compartment and extracellular space is presented. In Effect of NKCC and nonselective pathway, we have a glimpse of the effect of the glial membrane conductance changes as well as variations in the pia mater boundary conditions. We introduce the Na-K-Cl cotransporter (NKCC) channel into the glial membrane and a nonselective pathway on the pia mater and compare the potassium clearance with the baseline model. The NKCC channels on the glial membrane increase potassium clearance efficiency. An additional nonselective pathway in the pia mater does not have significant effect on potassium clearance because of the limited surface area of the pia mater.

Alternative distribution of stimulus location

In this section, current is applied at several different radial locations. We wondered whether the choice of radial location would change our calculations of potassium clearance and fluid velocity. This approach is used for many variables to crudely estimate the sensitivity of our results to assumptions.

To facilitate the discussion of the interaction between the extracellular pathway and the glial transmembrane pathway for K^+ clearance, we define the following regions that potassium flux could pass through:

- M_S, glial membrane in stimulated region;
- E_T, extracellular pathway on transition interface;
- M_{NS}, glial transmembrane in nonstimulated region; and
- G_T, glial pathway on transition interface.

The normal directions on M_S and M_{NS} point to extracellular space, and the normal direction of E_T and G_T is the radial direction. We mainly focus on the two particular periods of time: 1) during a train of axon firing ([0, T_{sti}]) and 2) after axon firing ([T_{sti}, T_{af}]) after the axon stimulation stops. In the simulations below, we take $T_{sti} = 0.2$ s and $T_{af} = 10$ s. The frequency of the stimuli is 50 Hz ($T = 0.02$ s), and each single stimulus has current strength $I_{sti} = 3 \times 10^{-3}$ A/m^2 with duration 3 ms.

Inner and outer radial regions stimulated. We first make a comparison between the inner radial region stimulated case, in which the current is applied at $z = z_0$ (= 2.25 mm) cross section $S_{sti}^{in}\left(= \left\{(r,z)\middle| r < \frac{R_a}{2},\ z = z_0\right\}\right)$, and the outer radial region stimulated case, in which $S_{sti}^{out}\left(= \left\{(r,z)\middle| \frac{R_a}{2} < r < R_a,\ z = z_0\right\}\right)$. Because the axon signal propagates in the z

Please cite this article in press as: Zhu et al., A tridomain model for potassium clearance in optic nerve of *Necturus*, Biophysical Journal (2021), https://doi.org/10.1016/j.bpj.2021.06.020

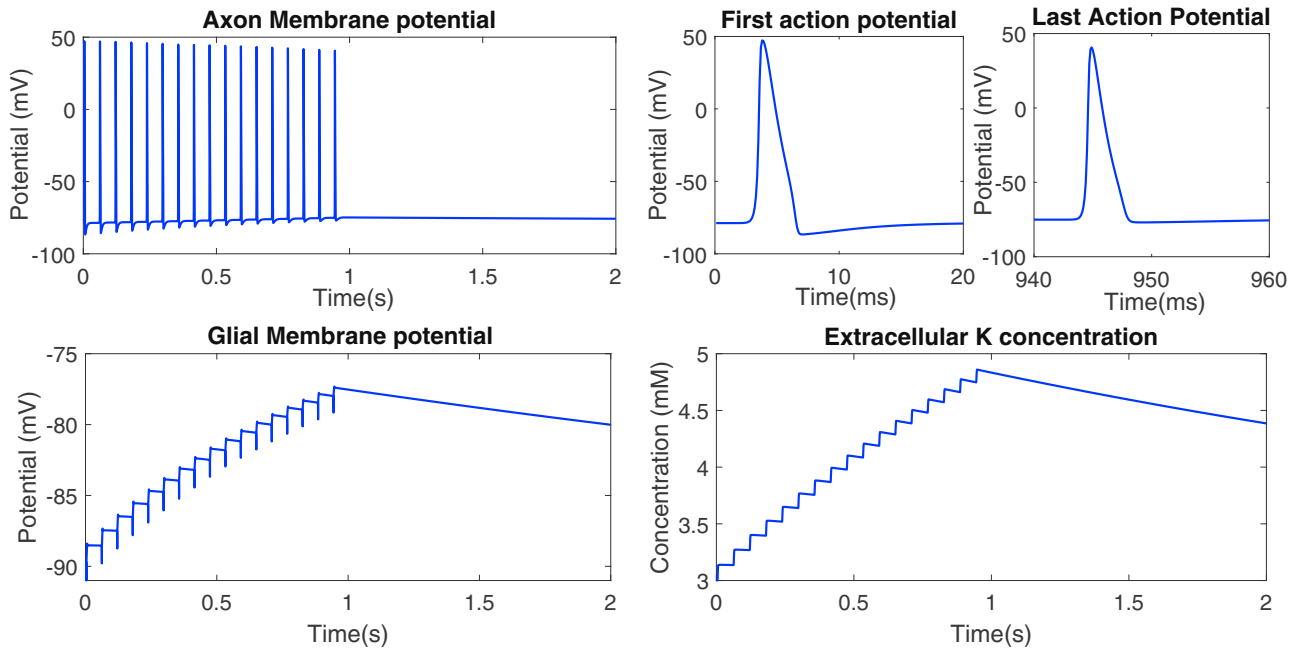

FIGURE 4 Recording axon membrane potential, glial membrane potential, and extracellular K^+ at center axis point (where $r = 0$ and $z = L/2$) when using the extracellular solution with 3 mM K^+. To see this figure in color, go online.

direction, for the inner radial region stimulated case, the stimulated region is $V_S^{in} = \left\{(r,z)\middle| r < \frac{R_a}{2}, z \in [0,L]\right\}$ and the nonstimulated region is $V_{NS}^{in} = \left\{(r, z)\middle|\frac{R_a}{2} < r < R_a,\ z \in [0,L]\right\}$; for the outer radial region stimulated case, $V_S^{out} = V_{NS}^{in}$ and $V_{ns}^{out} = V_s^{in}$. The transition interface $S_{sti} = \{(r,z)|r = \frac{R_a}{2}, z \in [0,L]\}$ is the same for both cases.

During a train of neuron firing. In Fig. 6, we show the total potassium flux (potassium flux density integrated over area) and cumulative potassium flux (total potassium flux integrated over time) during the axon firing period $[0, T_{sti}]$. In both cases, the figures show that the transmembrane flow from extracellular to glial and the communication inside the extracellular act together to help the potassium clearance. The strength of fluxes is gradually increased during axon firing period as in Fig. 6, *a and b*. The results confirm that the potassium flux during stimulus flows from the stimulus region to the nonstimulus region in both the extracellular space and glial compartment. The cumulative potassium flux through the glial membrane (M_S) is twice as large as that through the extracellular pathway in the transition interface (E_T) as shown in Fig. 6, *e and f*.

The glial compartment serves as an important and quick potassium transport device to remove potassium accumulated while the neuron fires action potentials. In the stimulated region, the accumulated potassium makes the potassium Nernst potential more positive. The change in the potassium Nernst potential induces potassium movement into the glial compartment from the extracellular space (Fig. 6 *a*). This inflow makes the glial compartment electric potential more positive and moves potassium ions from the stimulated region to the unstimulated region (Fig. 6 *d*). In the unstimulated region, the glial membrane potential also becomes more positive, as it does in the stimulated region, because the glia is an electrical syncytium in the longitudinal and radial directions. However, the glial potassium Nernst potential in the unstimulated region is not very different from that in the

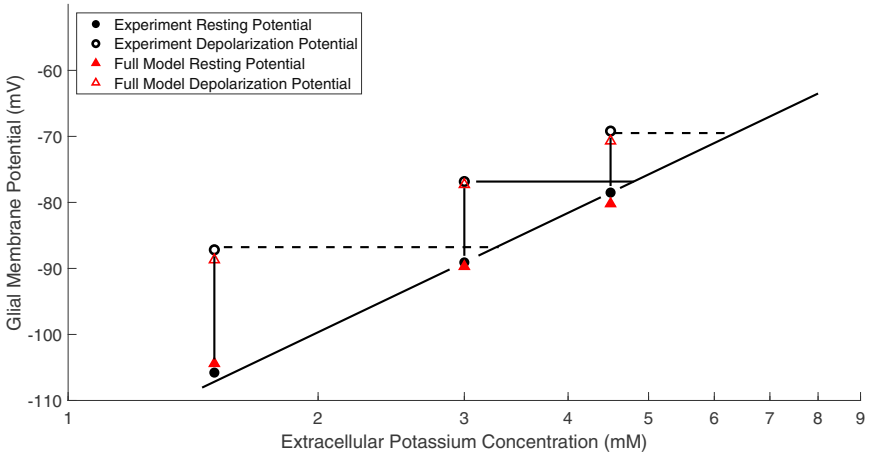

FIGURE 5 Comparison between the experiment in (8) and simulation on the effect of nerve impulses on the membrane potential of glial cells. The solid symbols are resting potentials, and the open symbols are depolarization potentials with different K^+ concentrations in Ω_{ex}^{OP}. To see this figure in color, go online.

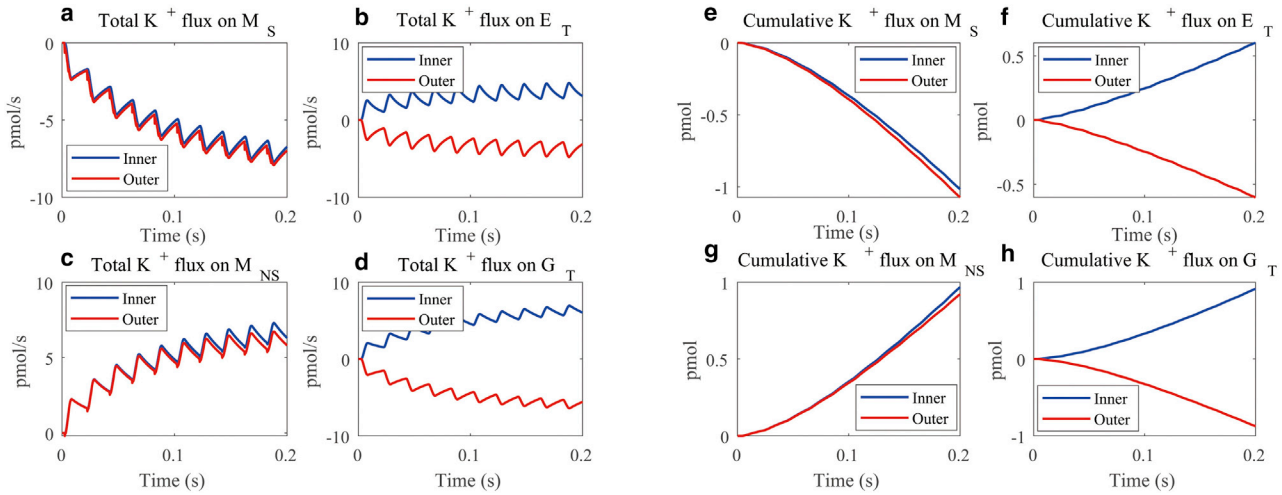

FIGURE 6 (*a–d*) Potassium flux through M_S, E_T, M_{NS}, and G_T during a train of axon firing. (*e–h*) Cumulative potassium flux during axon firing period [0, T_{sti}]. To see this figure in color, go online.

resting state. These potentials produce the outward potassium flux from the glial compartment in the unstimulated region (Fig. 6 *c*). Interacting regions of this sort depend on spatial variables and the properties of the glia as a syncytium in the longitudinal as well as radial directions. It is difficult to capture these effects in models that do not include radial and longitudinal directions as independent variables. Compartment models are possible, but it is very difficult to uniquely define invariant parameters over the range of conditions of interest. If additional information becomes available experimentally, the "new" conductances and pumps cannot be introduced in a unique way, without much thought. As the model is adapted to other structures in the brain, the parameters of a compartment model become quite difficult to specify. The distributed model uses structurally defined parameters with structural or specific biophysical meaning. These can be adjusted in a reasonably specific way in different versions of this model, appropriate for different systems in the brain. The schematic graph of potassium circulation in the optic nerve is summarized in Fig. 10 *a*.

The spatial distributions of K^+ concentration changes from resting state over time are shown in Figs. 7 and 8. Fig. 7 shows that the K^+ concentration varies in the stimulus region along the longitudinal direction during one action potential, whereas there is no change of K^+ in the nonstimulus region. Fig. 8, *a and b* show there is an obvious potassium concentration difference in the radial direction after a train of stimuli over time $T_{sti} = 0.2$ s. In Fig. 8 *c*, the potassium concentration difference vanishes because of the communication of the extracellular space and glial compartment shown in Fig. 11, *f and g* during an action potential.

The water circulation in the optic nerve is driven by the gradient of osmotic pressure in the stimulated region. In the stimulated region, the extracellular osmotic pressure k_BTO_{ex} decreased, and the glial compartment osmotic flow of water is increased. This is because there is more potassium flux moving into the glial compartment through the glial membrane but a smaller amount of sodium flux out of the glial compartment because of the ion channel conductance difference between the potassium and sodium channels in the glial membrane. In the glial compartment in the stimulated region of the optic nerve fiber, there is an increase in the water flux into the glial compartment from the extracellular space (Fig. 9 *a*). The volume fraction of the glial compartment and the hydrostatic pressure have also increased. The increased hydrostatic pressure in the stimulated region also raises the hydrostatic pressure in locations far away from the stimulated region. The increased pressure also drives the flow from stimulated region to the unstimulated region because the glial compartment is a connected space (Fig. 9 *d*), a longitudinal syncytium. In the unstimulated region, the water flows out of the glial compartment into the unstimulated region because of the increased hydrostatic pressure in the glial compartment (Fig. 9 *c*). Then, because the fluid is incompressible, the fluid in the unstimulated region flows back to the stimulated region (Fig. 9 *b*). The schematic graph of water circulation in the optic nerve is summarized in Fig. 10 *b*. This is a summary of our results. It is not a compartment model. Our models are distributed.

In Fig. 9, *e and f*, we show the volume change of extracellular space. In the stimulated region, the extracellular space decreases because the water flows into the glial cell, whereas in the unstimulated region, the extracellular space swells because of spatial buffering water flow (61).

In sum, during a train of action potentials in the axon, the potassium flux transport pattern and potassium flux strength across the glia membrane and through the extracellular pathway are the same for both radial regions, inner and outer. The glial compartment pathway is the dominant clearance mechanism of the potassium accumulated in the extracellular stimulated region in both cases.

After axon firing period. After the stimulus period, the main potassium clearance mechanism is the passive flow from extracellular space to glial compartment through the glial membrane. The potassium flux in the extracellular region and glial compartment is negligible. In these calculations, the extracellular region and the glial compartment could be approximated as a single compartment. We show a schematic figure of potassium flux pattern in Fig. 13 *a*. This is a summary and sketch of our results. We did not use a compartment model. Our model is distributed.

In Fig. 11, we show the total potassium flux and cumulative potassium flux through M_S, E_T, M_{NS}, and G_T after axon firing period [T_{sti}, T_{af}]. For both cases, the strength of potassium fluxes through the glial transmembrane pathway (M_S) and extracellular pathway has dramatically decreased after the axon stopped firing.

Fig. 11 *e* shows that in both cases (inner stimulus and outer stimulus), the potassium flows into the stimulated glial compartment after the axon firing period. Fig. 11 *g* shows that the potassium flux through the glial membrane in the nonstimulated region reverses its direction for a short time after axon stop firing. This occurs because the extracellular potassium concentration becomes evenly distributed in both the stimulated and nonstimulated extracellular space.

In Fig. 11 *f*, in the extracellular space, potassium flows back to the stimulus region from the nonstimulus region via the extracellular pathway (in both cases). Accordingly, Fig. 12 shows that after the axon stops firing, the water flow inside the compartments becomes almost zero. The water flows through both stimulated and unstimulated glial membrane into the glial compartment, which is the same as the schematic graph Fig. 13 *b*.

In sum, after the axon stops firing action potentials, the extracellular potassium concentration is quickly transported in the glial compartment and

Please cite this article in press as: Zhu et al., A tridomain model for potassium clearance in optic nerve of *Necturus*, Biophysical Journal (2021), https://doi.org/10.1016/j.bpj.2021.06.020

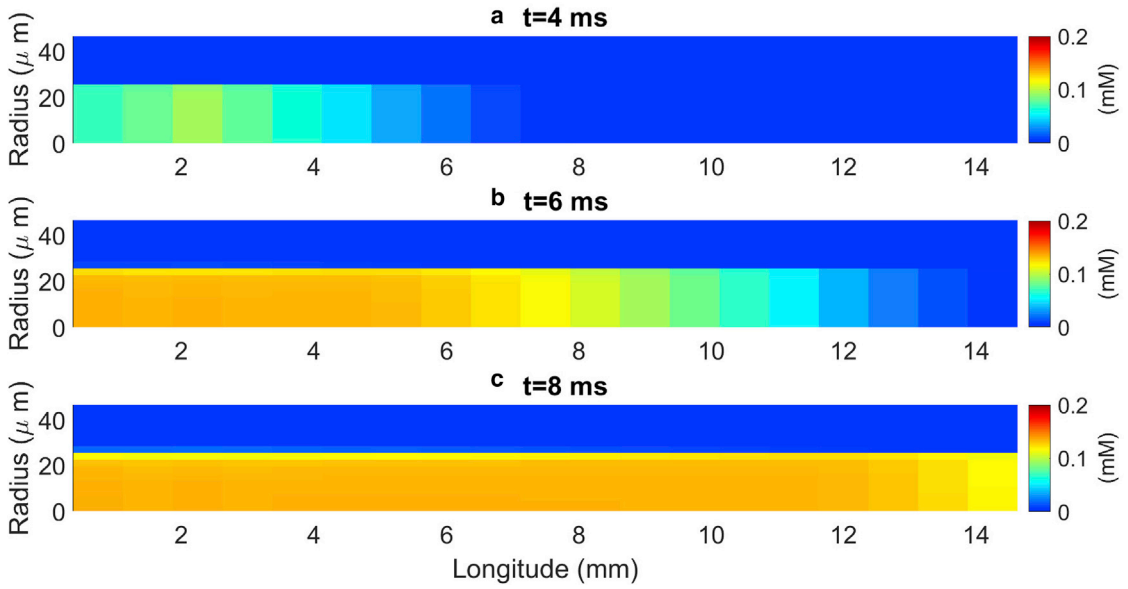

FIGURE 7 Spatial distribution of potassium changes from the resting state. To see this figure in color, go online.

extracellular pathway. The main clearance of potassium is through the glia membrane in both stimulated and unstimulated regions. The potassium flux through the extracellular pathway becomes weaker after the axon stops firing action potentials.

In Fig. 14, *a and b*, we show the variation of the potassium concentration in the extracellular stimulated and unstimulated regions, respectively. The peak potassium concentration in the stimulated region is higher in the outer stimulated case compared to the inner stimulated case. As discussed previously, the strength of potassium clearance is the same for both cases, whereas in the outer radial stimulated case, there is three times as much potassium in the extracellular space during the axon firing as in the inner radial stimulated case.

The equality of potassium clearance in both cases also explains why the potassium concentration drops faster in the inner radial stimulated case than the outer one after axon stop firing. We provide a decay timetable in the Supporting materials and methods.

Randomly distributed stimulation. Spatially uniform patterns of stimulation might produce systematic artifacts as occur in Moire patterns and aliasing. In this section, we study whether random stimulation patterns in space differ from spatially uniform patterns. We apply a train of stimuli to four randomly distributed stimulated regions in the radial direction. The strength and duration of the stimulus is same as in the Inner and outer radial regions stimulated, and the current is applied at the same longitudinal

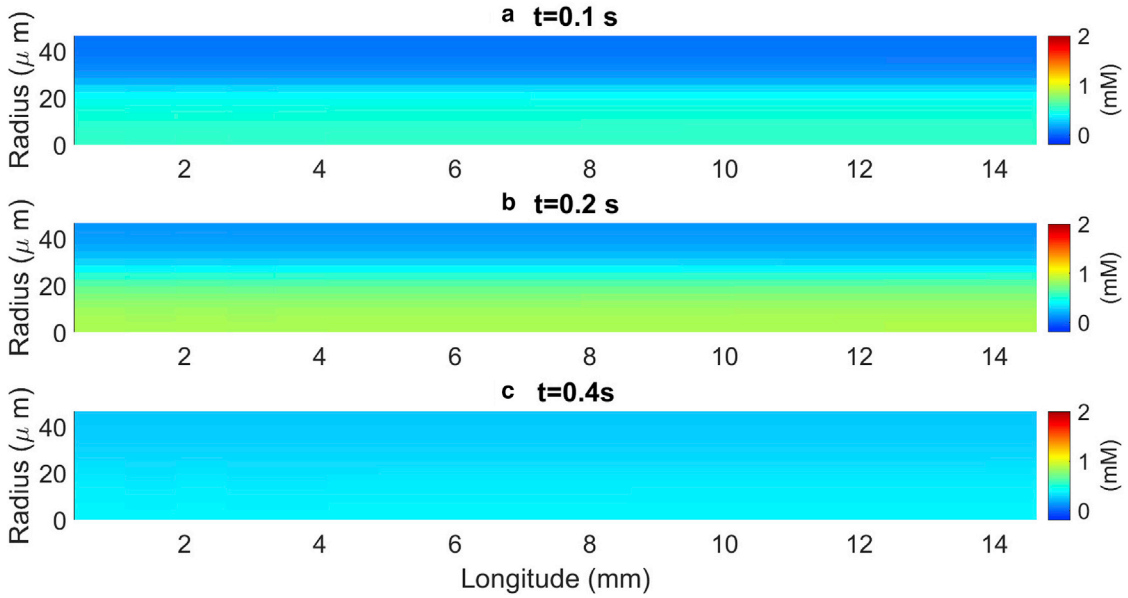

FIGURE 8 Spatial distribution of potassium changes from the resting state during and after a train of stimuli. To see this figure in color, go online.

Please cite this article in press as: Zhu et al., A tridomain model for potassium clearance in optic nerve of *Necturus*, Biophysical Journal (2021), https://doi.org/10.1016/j.bpj.2021.06.020

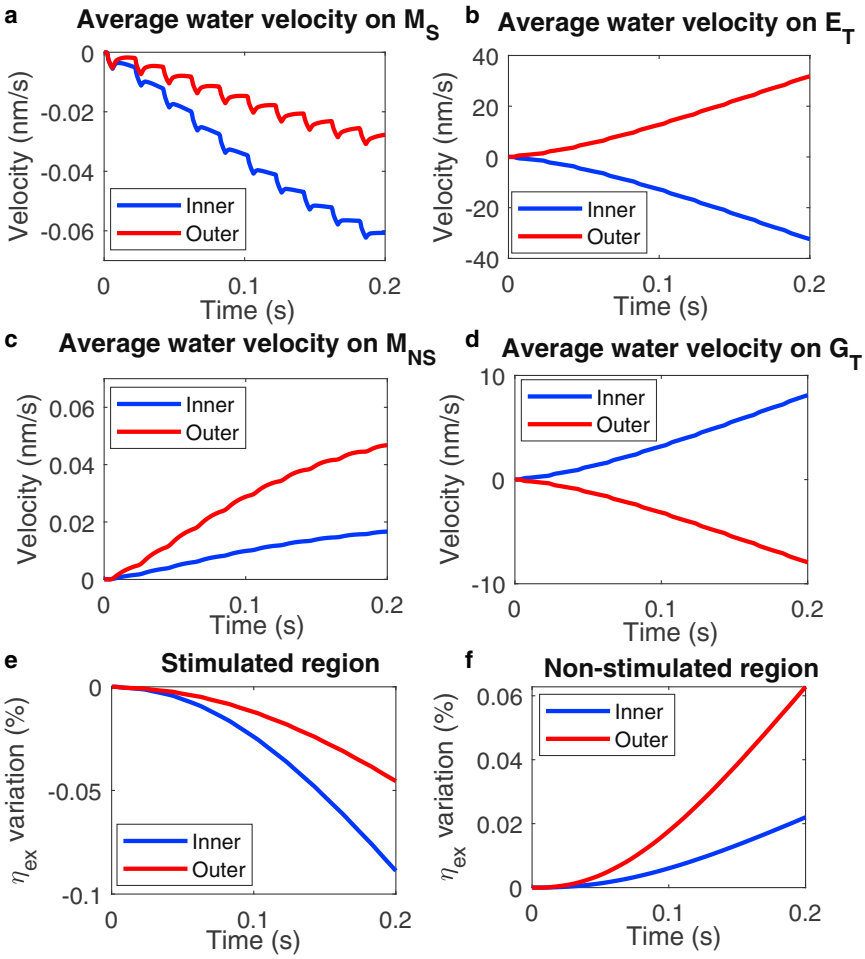

FIGURE 9 (*a–d*) Average water velocity through M_S, E_T, M_{NS}, and G_T during a train of axon firing period [0, T_{sti}]. (*e* and *f*) The extracellular volume fraction variation in the stimulated region and nonstimulated region. To see this figure in color, go online.

location ($z = z_0$). The details of the radial stimulated location in each case are shown in Fig. 15.

During a train of axon firing. We compare the spatially random stimulated case (case 1; the rest of the cases are similar and shown in the Supporting materials and methods) with the inner radial region stimulated case in Fig. 16, *a–d*. During a train of axon firing, Fig. 16, *a and b* show, in the randomly stimulated case, that the potassium clearance through the glial transmembrane (M_S) has been reduced, whereas the potassium flux through extracellular pathway in transition interface (E_T) has dramatically increased. Fig. 16, *e and f* show that the major clearance pathway in the randomly stimulated cases becomes the extracellular pathway in transition interface (E_T). More potassium flux goes through the extracellular path in the transition interface in comparison to how much goes through glial membrane in the stimulated region. This differs from the outer and inner stimulated cases, in which the glial transmembrane (M_S) dominates, as seen in Fig. 6, *e and f*.

Fig. 16, *a–d* show that in the inner stimulated case (*blue line*), the potassium flux strength gradually increased with small oscillation in each axon stimulus time period, whereas in the spatially random stimulated case (*red line*), the potassium flux strength shows a periodic pattern in time with larger oscillation in each stimulus period. The reason for this quite different potassium flux pattern is that the extra potassium in the extracellular stimulated region has been cleared quicker in the random selected case. So, in each stimulus period, the potassium flux decreases dramatically because the potassium goes back to its resting state, whereas in the inner stimulus case, for each stimulus period, the clearance of potassium is slower and there is accumulation of potassium in the stimulated extracellular space.

In sum (Fig. 16, *e and f*), during a train of axon firing, much more potassium flux goes through the extracellular pathway through transition interface (E_T), which reduces the effect of glial compartment pathway in the stimulated region (M_S).

After axon firing period. After the axon stops firing action potentials, both the spatially random case and the uniform inner case have similar reduced potassium fluxes (see M_S, E_T, M_{NS}, and G_T in Fig. 17, *e and g*) and show that the main pathway for potassium clearance (after the action potentials cease) is through the glial transmembrane pathway.

Fig. 17 *h* shows a large difference between the spatially random and the spatially uniform case in some properties as we feared might occur. The cumulative transport of potassium flux through the glial compartment transition interface in the spatially random cases is much smaller than it is in the uniform inner case. This is because during the axon firing period, the extracellular potassium in the stimulated region has been quickly removed in the random cases. The potassium concentration became more homogeneous, and there was less difference between the stimulated region and nonstimulated regions. As a result, the glial compartment electric potential ϕ_{gl} becomes homogeneous in entire glial compartment and the electric drift flow in the glial transition interface was reduced for potassium. These results show the importance of checking for artifacts produced by artificial assumptions of spatial uniformity or periodicity.

Potassium clearance and fluid velocity in the extracellular space and glial compartment. Because the potassium goes less through the glial transmembrane pathway in the stimulated region, the osmosis in the extracellular k_BTO_{ex} and in glial k_BTO_{gl}, and variation in the stimulated region has been reduced. Therefore, the strength of the velocities decreases in both glia and extracellular compartment because of the decrease of the glial transmembrane water flow as shown in Fig. 18, *c and d*. The average potassium concentration changes in both the stimulated region and

Please cite this article in press as: Zhu et al., A tridomain model for potassium clearance in optic nerve of *Necturus*, Biophysical Journal (2021), https://doi.org/10.1016/j.bpj.2021.06.020

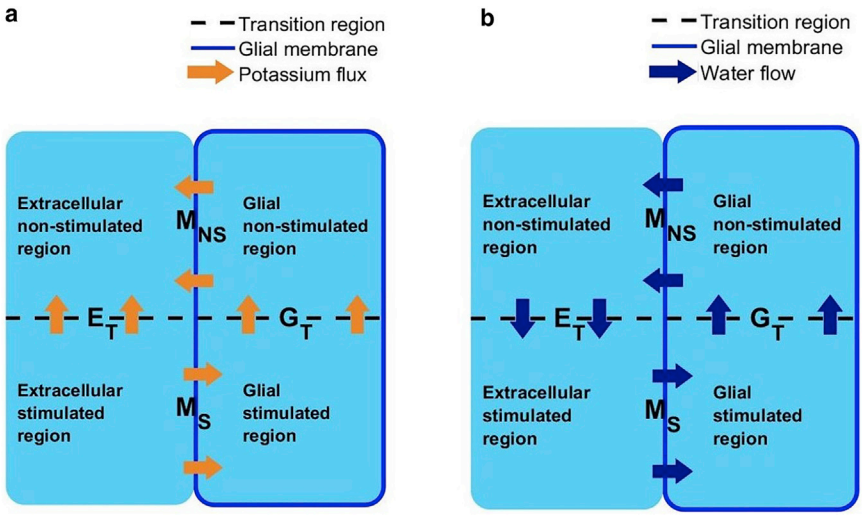

FIGURE 10 (*a*) Schematic graph of the potassium flux when axon is stimulated. In the stimulated region, the potassium moves through the extracellular pathway and through the glial compartment by way of the glial membrane. In the nonstimulated region, the potassium leaks out to the extracellular space through the glial membrane. (*b*) Schematic graph of the water circulation when the inner part of the axon is stimulated. In the stimulated region, the glial transmembrane water flow goes from extracellular space into the glial compartment as the effect of osmosis difference. In the extracellular space, water goes from the nonstimulated region to the stimulated region in the radial direction. In the glial compartment, it goes in the opposite direction. Note that these graphs summarize outputs of large numbers of calculations solving partial differential equations in longitudinal and radial spatial directions and time. They do not represent a compartmental model. They are the output of a model distributed in space. To see this figure in color, go online.

nonstimulated region as shown in Fig. 18, *a and b*, and its decay time in each case is in the Supporting materials and methods.

Effect of NKCC and nonselective pathway

In this section, we consider the effect of glial membrane conductance and a nonselective pathway on the pia boundary on the potassium clearance process. We first introduce the NKCC channel into the glial membrane, as widely studied in the literature. We compare simulation results between the model with NKCC and without NKCC. In the second part, we consider the effect of a nonselective pathway in the pia mater boundary. That pathway allows the convection flux through an extracellular pathway out of the optic nerve. We investigate how these factors affect the potassium clearance. Although the contribution of the NKCC channel is significant, it is important to realize that in our state of knowledge, other relevant channels may not yet have revealed themselves. Some channels become activated only under special conditions that are hard to find. Some channels may become activated only to protect systems under severe stress, as in clinical situations such as oxygen deprivation, swelling, and so on. It will be important to identify such channels as the model is applied to clinical situations, some of which are of considerable importance.

Effect of NKCC on the glial membrane. We introduce a model of NKCC channels in the glial membrane as in (29,62). We describe the K^+, Na^+, and Cl^- flux through the NKCC channel in the glial membrane as in (29,62):

$$J^{K}_{NKCC} = -\frac{I^{NKCC}_{\max}}{ez^{K}}\log\left(\frac{C^{K}_{ex}}{C^{K}_{gl}}\frac{C^{Na}_{ex}}{C^{Na}_{gl}}\left(\frac{C^{Cl}_{ex}}{C^{Cl}_{gl}}\right)^{2}\right),$$

$$J^{Na}_{NKCC} = -\frac{I^{NKCC}_{\max}}{ez^{Na}}\log\left(\frac{C^{K}_{ex}}{C^{K}_{gl}}\frac{C^{Na}_{ex}}{C^{Na}_{gl}}\left(\frac{C^{Cl}_{ex}}{C^{Cl}_{gl}}\right)^{2}\right), \qquad (28)$$

$$J^{Cl}_{NKCC} = 2\frac{I^{NKCC}_{\max}}{ez^{Cl}}\log\left(\frac{C^{K}_{ex}}{C^{K}_{gl}}\frac{C^{Na}_{ex}}{C^{Na}_{gl}}\left(\frac{C^{Cl}_{ex}}{C^{Cl}_{gl}}\right)^{2}\right).$$

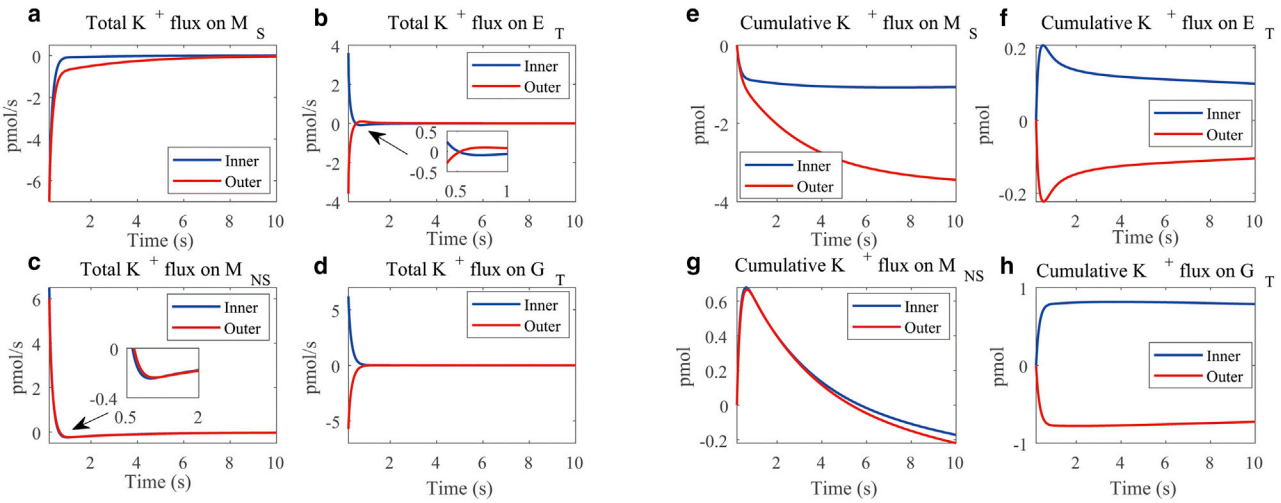

FIGURE 11 (*a–d*) Potassium flux through M_S, E_T, M_{NS}, and G_T after a train of action potentials. (*e–h*) Cumulative potassium flux after axon firing. To see this figure in color, go online.

Please cite this article in press as: Zhu et al., A tridomain model for potassium clearance in optic nerve of *Necturus*, Biophysical Journal (2021), https://doi.org/10.1016/j.bpj.2021.06.020

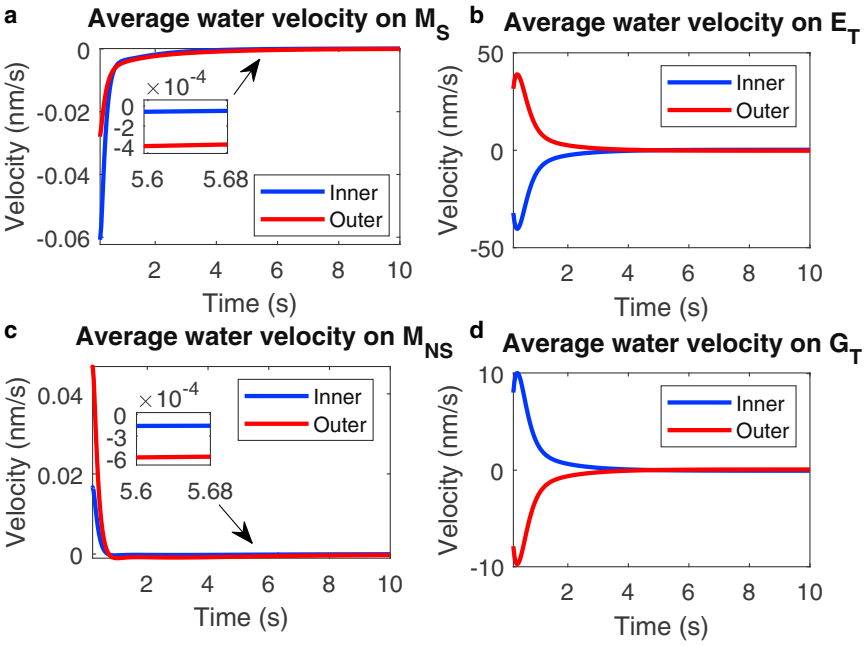

FIGURE 12 (*a–d*) Average water velocity through M_S, E_T, M_{NS}, and G_T after a train of axon firing. To see this figure in color, go online.

To compare the effect of NKCC without NKCC, we keep the potassium and sodium concentration, as well as the resting electric potential, in the glial compartment and extracellular space the same. In the resting state, we set sodium and potassium current through NKCC channel to be comparable with respect to the Na/K pump current as in the studies (29,62). In the Supporting materials and methods, we provide the two sets of parameters (NKCCa and NKCCb) that balance the additional NKCC current through the glial membrane.

In the simulation below, we compare the models with and without NKCC. The stimulated region (Fig. 19) shows the cumulative potassium flux through the M_S, E_T, M_{NS}, and G_T during and after stimuli.

Fig. 19 *a* shows that more potassium goes through the glial membrane in the simulated region during axon firing when NKCC is present, which is hardly surprising. The NKCC channel has enhanced the transport of potassium through the glial membrane after the axon stopped firing as in Fig. 19, *e and g*.

Fig. 20, *a and b* show the variation of potassium concentration in the extracellular space in the stimulated and unstimulated cases. The potassium decay in much faster when NKCC is present presumably because NKCC allows larger movement of potassium into the glial compartment. We provide the decay timetable in the Supporting materials.

The quicker potassium is taken into glial compartment by the NKCC, the slower the return of potassium concentration back to resting state. Fig. 20 *c* shows the variation of the potassium concentration in the stimulated region. After action potentials cease, the potassium movement back to the axon compartment is reduced in the model with NKCC channel. Fig. 20 *c* shows that the average potassium concentration in the baseline model increases faster after the axon stops firing than in the model with NKCC.

Nonselective pathway through the pia matter. In this section, we consider the effect of a nonselective pathway across the pia boundary. The nonselective pathway allows both ion and water fluid transport through the cleft between the cells in the pia mater. We assume that the water fluid going

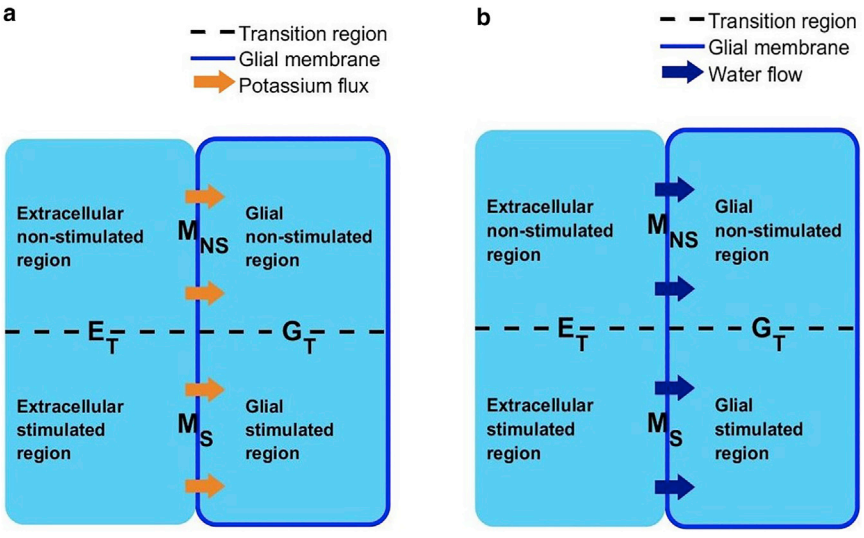

FIGURE 13 (*a*) Schematic graph of the potassium flux after the axon was stimulated. The potassium flux leaks into the glial compartment from the extracellular space through the glial membrane in both the stimulated and unstimulated regions. The potassium flux in the extracellular space and glial compartment is negligible. (*b*) Schematic graph of the water flux after the axon was stimulated. Note these graphs are graphs that summarize outputs of large numbers of calculations solving partial differential equations in longitudinal and radial spatial directions and time. They do not represent a compartmental model. They are the output of a model distributed in space. To see this figure in color, go online.

Please cite this article in press as: Zhu et al., A tridomain model for potassium clearance in optic nerve of *Necturus*, Biophysical Journal (2021), https://doi.org/10.1016/j.bpj.2021.06.020

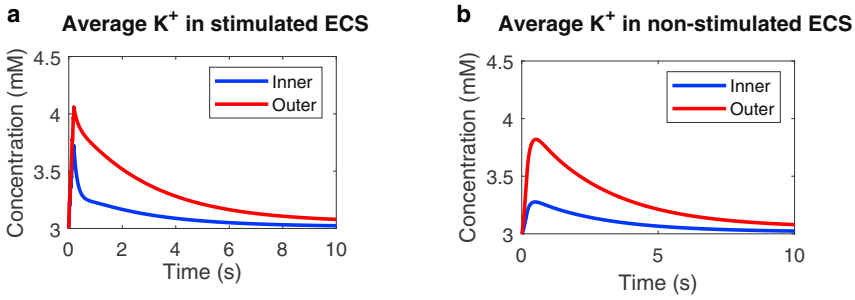

FIGURE 14 (*a* and *b*) Potassium concentration variation in the extracellular stimulated region and nonstimulated region. To see this figure in color, go online.

through the nonselective pathway only depends on the hydrostatic pressure difference. Therefore, the fluid condition on pia boundary (Γ_7) in (16) becomes

$$\boldsymbol{u}_{ex}^{OP}\cdot\widehat{\boldsymbol{r}} = \boldsymbol{u}_{ex}^{SAS}\cdot\widehat{\boldsymbol{r}} = u_{pia}^{m} + u_{pia}^{ns}, \quad \text{on } \Gamma_7,$$

where

$$u_{pia}^{m} = L_{pia}^{m}\left(p_{ex}^{OP} - p_{ex}^{SAS} - \gamma_{pia}k_BT\left(O_{ex}^{OP} - O_{ex}^{SAS}\right)\right)$$

and

$$u_{pia}^{ns} = L_{pia}^{ns}\left(p_{ex}^{OP} - p_{ex}^{SAS}\right).$$

The nonselective pathway between the cell clefts provides an additional pathway for diffusion (∇C_l^i), electric drift ($C_l^i\nabla\phi_l$), and convection for ions ($C_l^i\boldsymbol{u}_l$). We modify the boundary condition (24) for ion on pia boundary (Γ_7) as

$$\boldsymbol{j}_{ex}^{i,OP}\cdot\widehat{\boldsymbol{r}} = \boldsymbol{j}_{ex}^{i,SAS}\cdot\widehat{\boldsymbol{r}}$$

$$= \frac{G_{pia}^{i} + G^{ns}}{z^i e}\left(\phi_{ex}^{OP} - \phi_{ex}^{SAS} - E_{pia}^{i}\right) + c_{ex}^{i}u_{pia}^{ns}, \quad \text{on } \Gamma_7.$$

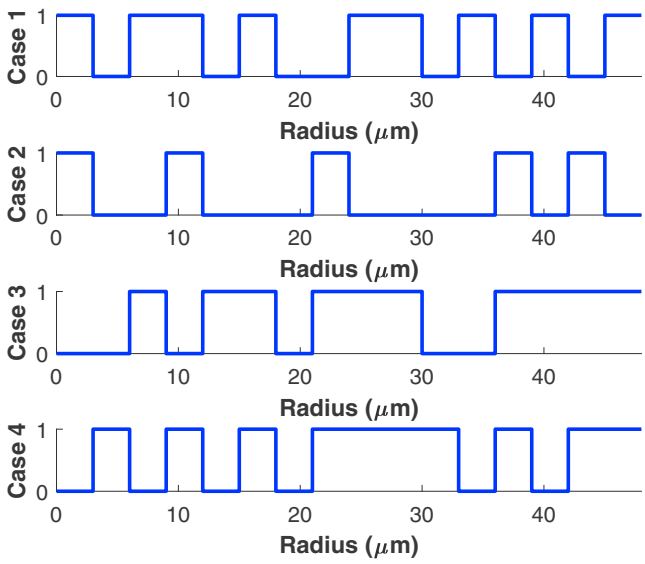

FIGURE 15 The stimulated radial segments in each case. The intervals with value 1 are stimulated segments, and the intervals with value 0 are unstimulated segments. To see this figure in color, go online.

Here, G^{ns} is the additional conductance due to the nonselective pathway and $C_{ex}^{i}u_{pia}^{ns}$ is the convection flux through the nonselective pathway on the pia boundary.

In the simulation below, we compare the model with a nonselective pathway with the model without the nonselective pathway. We choose the comparison parameter to be

$$\frac{G^{ns}}{G_{pia}^{K}} = \frac{L_{pia}^{ns}}{L_{pia}^{m}} = 10.$$

In Fig. 21, we show the potassium variation in extracellular space and the cumulative potassium flux through the pia mater and glial membrane.

The amount of potassium leak out of the optic nerve through the pia boundary is dramatically increased when the pathway is present in Fig. 21 *d*. However, the dominant pathway of potassium clearance is still through the glial membrane as previously in Fig. 21 *c*. This is because the total glial membrane area is much larger than the surface area on pia boundary,

$$\frac{2\pi R_a L}{V_{op}\mathcal{M}_{gl}} = O\left(10^{-3}\right),$$

where the V_on is the total optic nerve volume and M_gl is the glial membrane per unit volume. Fig. 21, *a and b* show that the nonselective pathway on the pia boundary does not accelerate the potassium clearance rate very much.

RESULTS AND DISCUSSION

There may be a concern about the large number of parameters in this and similar models. Models that contain large numbers of parameters can be difficult to compare and thus difficult to use in the scientific process of conjecture and refutation needed to understand these complex systems.

The need to deal with the complexity of the system as it is presented to us by evolution and used by animals should be clearly understood. Perhaps it is best understood by comparison with engineering systems. Engineering systems use enormous complexity—consider the 10^{13} components in our computers and their connections—to perform specific functions. If the complexity is not described in a model, the model cannot describe the functions. Biological systems perform definite functions and use structures to do so. They are often devices in the exact engineering sense of the word. Complexity is needed to define these systems because without that complexity, the systems do not function.

Of course, the complexity cannot be uniquely defined in either engineering or biological systems. One can always

Please cite this article in press as: Zhu et al., A tridomain model for potassium clearance in optic nerve of *Necturus*, Biophysical Journal (2021), https://doi.org/10.1016/j.bpj.2021.06.020

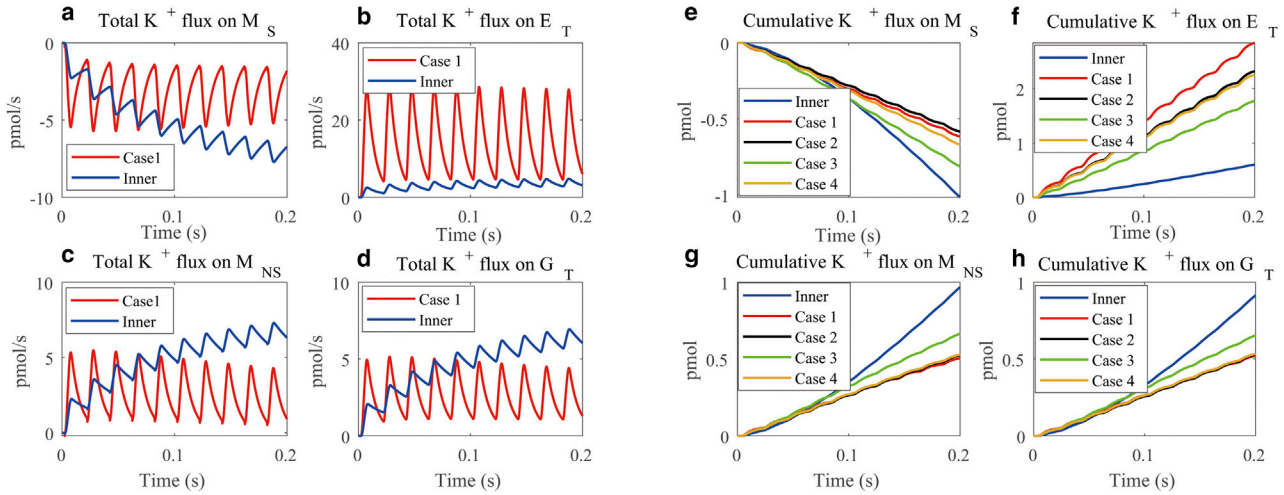

FIGURE 16 (*a–d*) The comparison between the spatially random stimulated case with the spatially uniform radial (inner) case during a train of axon firing. (*e* and *f*) The cumulative flux comparison in M_S, E_T, M_{NS}, and G_T during a train of axon action potentials. To see this figure in color, go online.

appeal to an atomic description in the desperation of ignorance, but it is not at all clear that much detail helps, and the problems of dealing with irrelevant thermal motion and difficulties in computation have made such an approach so difficult that it is rarely used in engineering. Here, we do the best we can by choosing structures and parameters that are needed considering their role in other similar biological systems.

The work here is done in the spirit of the structural analysis of physiological problems started by Falk and Fatt (63), continued by their student Eisenberg and his colleagues (64,65) and applied to the lens of the eye with Rae and Mathias. This approach uses measured anatomical parameters (best by application of statistical sampling methods to biological systems, which was pioneered by Eisenberg and then extended generally by Brenda Eisenberg (66)), and impedance spectroscopy (67), to determine parameters exploiting the invariance of the capacitance (per unit area) of biological membranes. Mathias and his group showed how to extend these methods to include water flow (68–70) in a bidomain tissue, the lens of the eye. We extend that structural approach here to a tridomain model of an optic nerve.

In the electrical case, the parameters of a structural model are quite well specified by this approach. When dealing with water flow, it is important to include measurements of flow and pressure. In our situation, the electrical information is available from the enormous knowledge of the properties of nerve fibers and action potential conduction developed since Hodgkin showed (71) that nerve conduction is

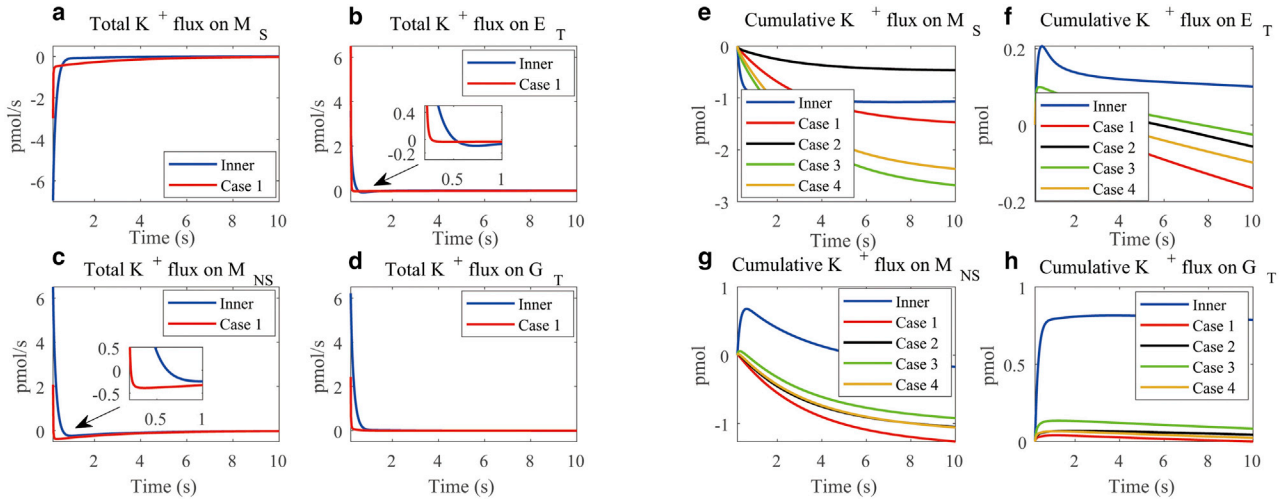

FIGURE 17 (*a–d*) The comparison between the spatially random case with the uniform inner radial case after a train of action potentials. Vector directions are as defined previously. (*e* and *f*) The cumulative flux comparison in M_S, E_T, M_{NS}, and G_T after a train of action potentials. To see this figure in color, go online.

Please cite this article in press as: Zhu et al., A tridomain model for potassium clearance in optic nerve of *Necturus*, Biophysical Journal (2021), https://doi.org/10.1016/j.bpj.2021.06.020

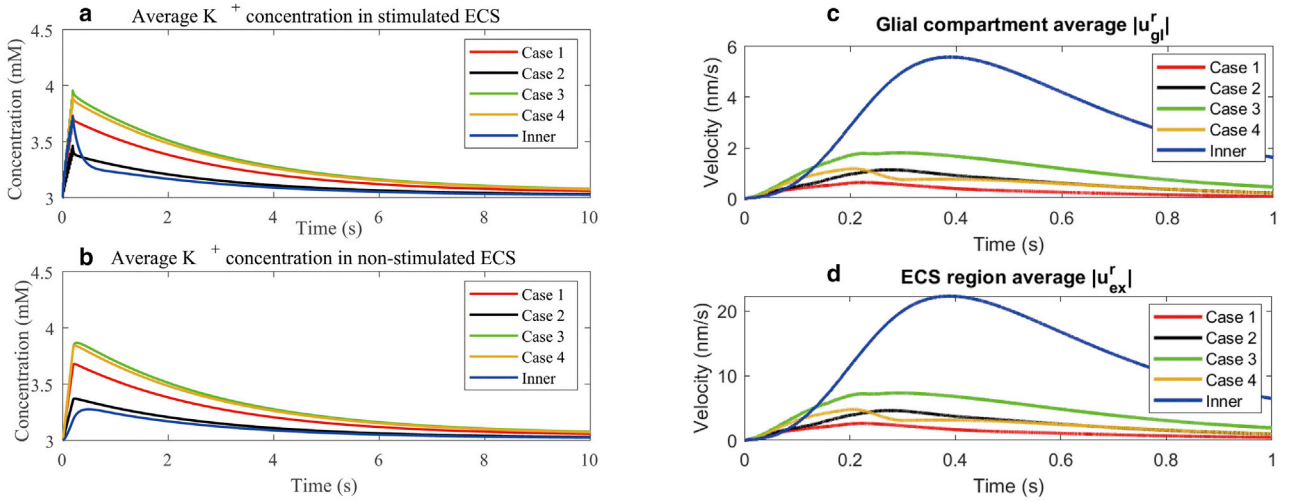

FIGURE 18 (*a* and *b*) Variation of potassium concentration in the extracellular simulated region and unstimulated regions. (*c* and *d*) Average glial compartment radial absolute velocity and extracellular space radial absolute velocity. To see this figure in color, go online.

electrical and not chemical (72). Measurements of pressure and flow are not available, and they are surely needed if the model is to be further refined or extended to other analogous systems of the central nervous system of great clinical importance. Measurements of a crucial property modified by water flow are possible thanks to the work of the Harvard group (Orkand et al. (8)). That work allows us to define our system as well as we have, but surely not well enough.

Because this work is developed to become a model of the important phenomena of the recently discovered glymphatic system (20,21), measurements of flow and pressure, as well as stereological measurements of structure and biophysical measurements of channel and pump distribution, will assume crucial importance in our view. Extensions of our theory and appropriate simplifications will also be helpful.

CONCLUSIONS

In this work, we propose a tridomain model to study potassium clearance in the optic nerve of Necturus in a series of experiments from Richard Orkand and the Harvard group (7,8). Our model, analysis, and simulations provide a detailed picture of the role of glial cells in buffering the concentration of ions, mostly in the narrow extracellular space. As the nerve axons are being stimulated, both the extracellular space and glial cells play important roles. They both clear extra potassium from the narrow extracellular space while the axon is firing action potentials. After the action potentials stop, the potassium remaining in the extracellular space is cleared by the glial compartment.

Our model shows that the longitudinal electrical syncytium of the glial cells is critical for clearing potassium

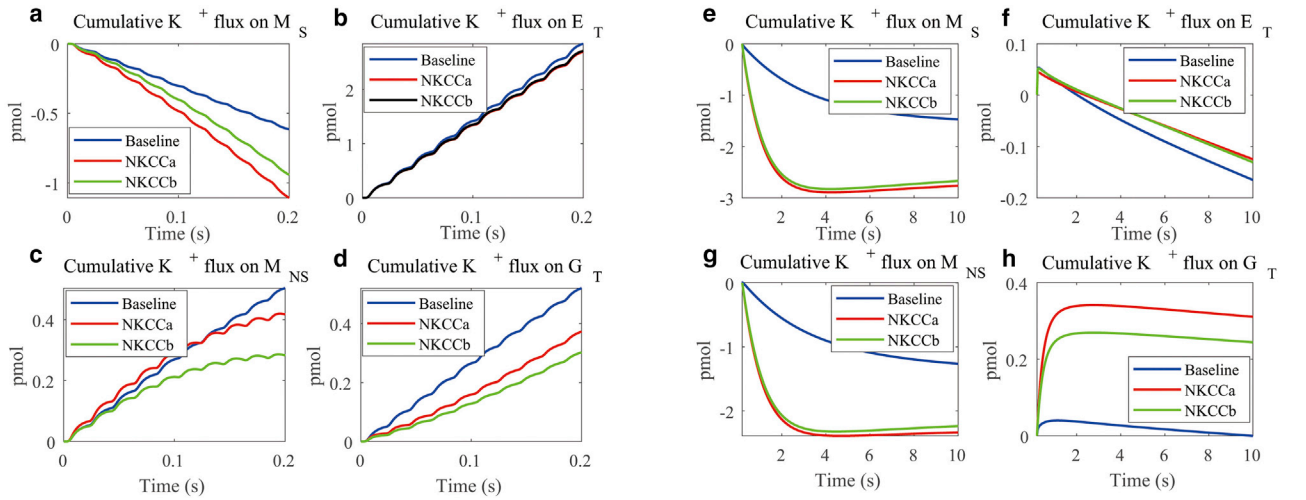

FIGURE 19 (*a–d*) The cumulative flux comparison in M_S, E_T, M_{NS}, and G_T during a train of action potentials. (*e–h*) The cumulative flux comparison in M_S, E_T, M_{NS}, and G_T after a train of action potentials. To see this figure in color, go online.

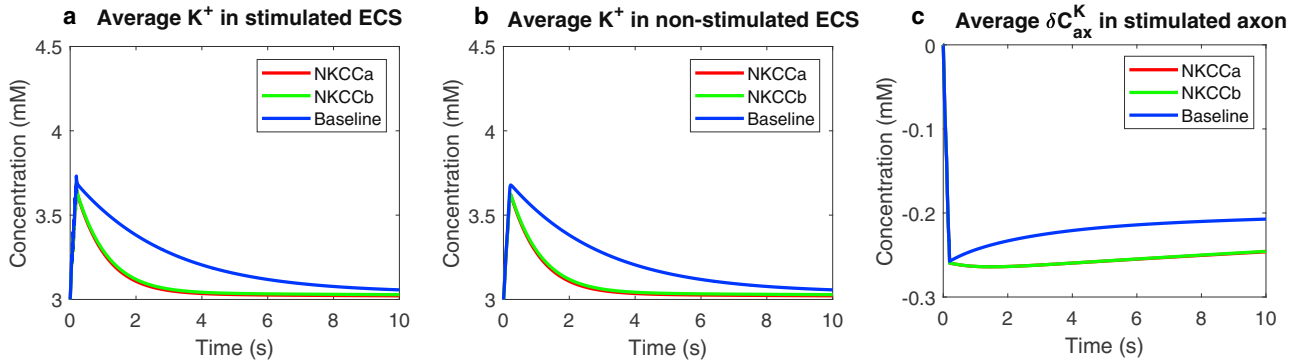

FIGURE 20 (*a* and *b*) Extracellular potassium concentration variation comparison between the model with NKCC and baseline model (without NKCC). (*c*) Average potassium variation in the axon stimulated region. To see this figure in color, go online.

(from the extracellular space) when the neuron fires. The inward glial transmembrane potassium flux in the stimulated region is almost the same as the outward potassium flux out to the extracellular space in the nonstimulated region in response to the change in potassium concentration between the extracellular space in the stimulated and unstimulated regions. This is because the electric potential spreads through the connected cells in the glial compartment. The glial electric potential in the unstimulated region becomes more positive in response to the depolarization of the glial electric potential in the stimulus region. The "syncytial properties" of the glial compartment are a feature that separates our field model with its partial differential equations from the compartment models in the literature that use ordinary differential equations. Compartment models lack the combination of space and time dependence needed to describe the temporal and spatial spread of potential. The combined temporal and spatial spread of potential is a crucial property of neurons. Here, we show that the combined temporal and spatial spread of potential is a crucial property of the glia and the narrow extracellular space between glia and neurons. In a sense, we extend the electrical cable theory used to describe the spatial spread of the electrical potential of neurons to a theory of spatial distribution of flow in neurons, glia, and the narrow extracellular space between them.

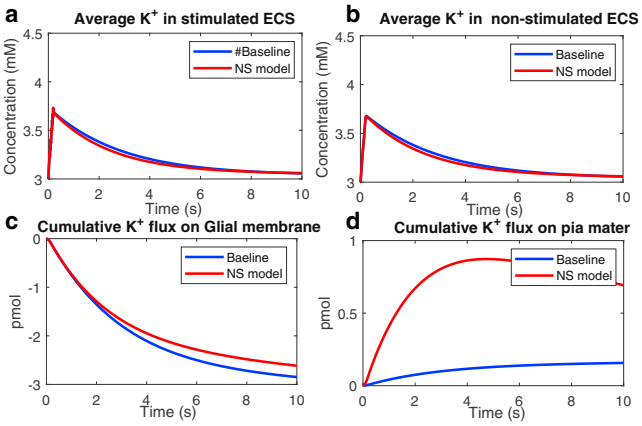

FIGURE 21 (*a* and *b*) Extracellular potassium concentration variation comparison between the model with nonselective pathway on pia boundary and baseline model (without nonselective pathway). (*c*) Total cumulative potassium flux through glial membrane. (*d*) Total cumulative potassium flux through pia boundary. To see this figure in color, go online.

We discuss the effect of enhanced potassium conductance in the glial membrane and nerve membranes of the pia mater. On the one hand, incorporating NKCC channels into the glial membrane increases potassium clearance. Potassium clearance time is much shorter than that predicted by the baseline model (without NKCC channels in the glial membrane). On the other hand, an additional nonselective pathway in another location—in the pia mater—does not have a significant effect on potassium clearance. This is not surprising because the total membrane area of the glial membrane in the optic nerve is much greater than the effective surface membrane of nerves in the pia mater.

Finally, our analysis of the model for the optic nerve is just a first small step toward the understanding of the mechanisms of the glial compartment buffering effect during the potassium clearance and microcirculation patterns of water and ions. The axons considered here is without a myelin sheath. Myelin can be included by combining the model of myelinated nerve proposed in (58) as a first next step. Our distributed model and its partial differential equations can be generalized to describe ionic and water transport in tissues with more complicated and heterogeneous structures and with glymphatic pathways connected to the circulatory system. We expect that the spatially nonuniform distribution of ion and water channels and transporters will be used in many structures in the central nervous system to control flow. Obviously, at higher resolution, much more detailed experimental observations and structure measurements (such as pump distributions and membrane permeabilities) will be needed.

SUPPORTING MATERIAL

Supporting material can be found online at https://doi.org/10.1016/j.bpj.2021.06.020.

Please cite this article in press as: Zhu et al., A tridomain model for potassium clearance in optic nerve of *Necturus*, Biophysical Journal (2021), https://doi.org/10.1016/j.bpj.2021.06.020

AUTHOR CONTRIBUTIONS

Y.Z., S.X., and H.H. did the model derivations and carried out the numerical simulations. R.S.E. and H.H. designed the study, coordinated the study, and commented on the manuscript. All authors gave final approval for publication.

ACKNOWLEDGMENTS

This research is supported in part by National Natural Science Foundation of China, China, No. 12071190 (S.X.), the Fundamental Research Funds for the Central Universities, China (S.X.), the Fields Institute for Research in Mathematical Science (S.X., R.S.E., and H.H.), and the Natural Sciences and Engineering Research Council of Canada, Canada (H.H.).

SUPPORTING CITATIONS

References (73–76) can be found in the Supporting material.

REFERENCES

1. Hodgkin, A. L., A. F. Huxley, and B. Katz. 1952. Measurement of current-voltage relations in the membrane of the giant axon of Loligo. *J. Physiol.* 116:424–448.
2. Hodgkin, A. L., A. F. Huxley, and B. Katz. 1949. Ionic currents underlying activity in the giant axon of the squid. *Arch. Sci. Physiol. (Paris).* 3:129–150.
3. Hodgkin, A. L., and A. F. Huxley. 1952. Currents carried by sodium and potassium ions through the membrane of the giant axon of Loligo. *J. Physiol.* 116:449–472.
4. Frankenhaeuser, B., and A. L. Hodgkin. 1956. The after-effects of impulses in the giant nerve fibres of Loligo. *J. Physiol.* 131:341–376.
5. Hodgkin, A. L., and A. F. Huxley. 1952. A quantitative description of membrane current and its application to conduction and excitation in nerve. *J. Physiol.* 117:500–544.
6. Kuffler, S. W., and J. G. Nicholls. 1966. The physiology of neuroglial cells. *In* Ergebnisse der Physiologie Biologischen Chemie und Experimentellen Pharmakologie. Springer, pp. 1–90.
7. Kuffler, S. W., J. G. Nicholls, and R. K. Orkand. 1966. Physiological properties of glial cells in the central nervous system of amphibia. *J. Neurophysiol.* 29:768–787.
8. Orkand, R. K., J. G. Nicholls, and S. W. Kuffler. 1966. Effect of nerve impulses on the membrane potential of glial cells in the central nervous system of amphibia. *J. Neurophysiol.* 29:788–806.
9. Nedergaard, M., and S. A. Goldman. 2020. Glymphatic failure as a final common pathway to dementia. *Science.* 370:50–56.
10. O'Connell, R., and Y. Mori. 2016. Effects of glia in a triphasic continuum model of cortical spreading depression. *Bull. Math. Biol.* 78:1943–1967.
11. Tuttle, A., J. Riera Diaz, and Y. Mori. 2019. A computational study on the role of glutamate and NMDA receptors on cortical spreading depression using a multidomain electrodiffusion model. *PLoS Comput. Biol.* 15:e1007455.
12. Ayata, C., and M. Lauritzen. 2015. Spreading depression, spreading depolarizations, and the cerebral vasculature. *Physiol. Rev.* 95:953–993.
13. Wei, Y., G. Ullah, and S. J. Schiff. 2014. Unification of neuronal spikes, seizures, and spreading depression. *J. Neurosci.* 34:11733–11743.
14. Ullah, G., Y. Wei, …, S. J. Schiff. 2015. The role of cell volume in the dynamics of seizure, spreading depression, and anoxic depolarization. *PLoS Comput. Biol.* 11:e1004414.
15. Mori, Y. 2015. A multidomain model for ionic electrodiffusion and osmosis with an application to cortical spreading depression. *Physica D.* 308:94–108.
16. Miura, R. M., H. Huang, and J. J. Wylie. 2007. Cortical spreading depression: an enigma. *Eur. Phys. J. Spec. Top.* 147:287–302.
17. Gakuba, C., T. Gaberel, …, M. Gauberti. 2018. General anesthesia inhibits the activity of the "glymphatic system". *Theranostics.* 8:710–722.
18. Jiang, Q., L. Zhang, …, Z. Zhang. 2017. Impairment of the glymphatic system after diabetes. *J. Cereb. Blood Flow Metab.* 37:1326–1337.
19. Abbott, N. J., M. E. Pizzo, …, R. G. Thorne. 2018. The role of brain barriers in fluid movement in the CNS: is there a 'glymphatic' system? *Acta Neuropathol.* 135:387–407.
20. Jessen, N. A., A. S. F. Munk, …, M. Nedergaard. 2015. The glymphatic system: a beginner's guide. *Neurochem. Res.* 40:2583–2599.
21. Mestre, H., Y. Mori, and M. Nedergaard. 2020. The brain's glymphatic system: current controversies. *Trends Neurosci.* 43:458–466.
22. Tuckwell, H. C., and R. M. Miura. 1978. A mathematical model for spreading cortical depression. *Biophys. J.* 23:257–276.
23. Postnov, D. E., L. S. Ryazanova, and O. V. Sosnovtseva. 2007. Functional modeling of neural-glial interaction. *Biosystems.* 89:84–91.
24. Chang, J. C., K. C. Brennan, …, J. J. Wylie. 2013. A mathematical model of the metabolic and perfusion effects on cortical spreading depression. *PLoS One.* 8:e70469.
25. Yao, W., H. Huang, and R. M. Miura. 2011. A continuum neuronal model for the instigation and propagation of cortical spreading depression. *Bull. Math. Biol.* 73:2773–2790.
26. Bellinger, S. C., G. Miyazawa, and P. N. Steinmetz. 2008. Submyelin potassium accumulation may functionally block subsets of local axons during deep brain stimulation: a modeling study. *J. Neural Eng.* 5:263–274.
27. Chen, K. C., and C. Nicholson. 2000. Spatial buffering of potassium ions in brain extracellular space. *Biophys. J.* 78:2776–2797.
28. Reichenbach, A., J.-U. Stolzenburg, …, L. Hertz. 1993. What do retinal Müller (glial) cells do for their neuronal 'small siblings'? *J. Chem. Neuroanat.* 6:201–213.
29. Østby, I., L. Øyehaug, …, S. W. Omholt. 2009. Astrocytic mechanisms explaining neural-activity-induced shrinkage of extraneuronal space. *PLoS Comput. Biol.* 5:e1000272.
30. Sibille, J., K. Dao Duc, …, N. Rouach. 2015. The neuroglial potassium cycle during neurotransmission: role of Kir4.1 channels. *PLoS Comput. Biol.* 11:e1004137.
31. Bellot-Saez, A., O. Kékesi, …, Y. Buskila. 2017. Astrocytic modulation of neuronal excitability through K^+ spatial buffering. *Neurosci. Biobehav. Rev.* 77:87–97.
32. Nicholson, C., and S. Hrabětová. 2017. Brain extracellular space: the final frontier of neuroscience. *Biophys. J.* 113:2133–2142.
33. Hou, R., Z. Zhang, …, N. Wang. 2016. Intracranial pressure (ICP) and optic nerve subarachnoid space pressure (ONSP) correlation in the optic nerve chamber: the Beijing Intracranial and Intraocular Pressure (iCOP) study. *Brain Res.* 1635:201–208.
34. Morgan, W. H., C. Balaratnasingam, …, D.-Y. Yu. 2016. Cerebrospinal fluid pressure and the eye. *Br. J. Ophthalmol.* 100:71–77.
35. Killer, H. E., G. P. Jaggi, …, A. Mironov. 2007. Cerebrospinal fluid dynamics between the intracranial and the subarachnoid space of the optic nerve. Is it always bidirectional? *Brain.* 130:514–520.
36. Band, L. R., C. L. Hall, …, A. J. Foss. 2009. Intracellular flow in optic nerve axons: a mechanism for cell death in glaucoma. *Invest. Ophthalmol. Vis. Sci.* 50:3750–3758.
37. Zhu, Y., S. Xu, …, H. Huang. 2019. A bidomain model for lens microcirculation. *Biophys. J.* 116:1171–1184.
38. Nicholson, C. 2001. Diffusion and related transport mechanisms in brain tissue. *Rep. Prog. Phys.* 64:815–884.
39. Filippidis, A. S., S. G. Zarogiannis, …, C. Hatzoglou. 2012. Permeability of the arachnoid and pia mater. The role of ion channels in the leptomeningeal physiology. *Childs Nerv. Syst.* 28:533–540.
40. Hayreh, S. S. 1984. The sheath of the optic nerve. *Ophthalmologica.* 189:54–63.

41. Hayreh, S. S. 2009. Ischemic optic neuropathy. *Prog. Retin. Eye Res.* 28:34–62.

42. Jonas, J. B., E. Berenshtein, and L. Holbach. 2003. Anatomic relationship between lamina cribrosa, intraocular space, and cerebrospinal fluid space. *Invest. Ophthalmol. Vis. Sci.* 44:5189–5195.

43. Xu, S., B. Eisenberg, …, H. Huang. 2018. Osmosis through a semipermeable membrane: a consistent approach to interactions. *arXiv*, arXiv:1806.00646 https://arxiv.org/abs/1806.00646.

44. Feher, J. J. 2017. Quantitative Human Physiology: An Introduction. Academic Press, Cambridge, MA.

45. Hua, Y., A. P. Voorhees, and I. A. Sigal. 2018. Cerebrospinal fluid pressure: revisiting factors influencing optic nerve head biomechanics. *Invest. Ophthalmol. Vis. Sci.* 59:154–165.

46. Lu, Y.-B., K. Franze, …, A. Reichenbach. 2006. Viscoelastic properties of individual glial cells and neurons in the CNS. *Proc. Natl. Acad. Sci. USA.* 103:17759–17764.

47. Feola, A. J., J. G. Myers, …, C. R. Ethier. 2016. Finite element modeling of factors influencing optic nerve head deformation due to intracranial pressure. *Invest. Ophthalmol. Vis. Sci.* 57:1901–1911.

48. Eisenberg, B., Y. Hyon, and C. Liu. 2010. Energy variational analysis of ions in water and channels: field theory for primitive models of complex ionic fluids. *J. Chem. Phys.* 133:104104.

49. Malcolm, D. T. K. 2006. A computational model of the ocular lens. ResearchSpace@ Auckland, PhD thesis.

50. Mathias, R. T. 1985. Steady-state voltages, ion fluxes, and volume regulation in syncytial tissues. *Biophys. J.* 48:435–448.

51. Wan, L., S. Xu, …, P. Sheng. 2014. Self-consistent approach to global charge neutrality in electrokinetics: a surface potential trap model. *Phys. Rev. X.* 4:011042.

52. Vaghefi, E., D. T. Malcolm, …, P. J. Donaldson. 2012. Development of a 3D finite element model of lens microcirculation. *Biomed. Eng. Online.* 11:69.

53. Pérez-Pinzón, M. A., L. Tao, and C. Nicholson. 1995. Extracellular potassium, volume fraction, and tortuosity in rat hippocampal CA1, CA3, and cortical slices during ischemia. *J. Neurophysiol.* 74:565–573.

54. McLaughlin, S., and R. T. Mathias. 1985. Electro-osmosis and the reabsorption of fluid in renal proximal tubules. *J. Gen. Physiol.* 85:699–728.

55. Gardiner, B. S., D. W. Smith, …, J. G. Crowston. 2010. Computational modeling of fluid flow and intra-ocular pressure following glaucoma surgery. *PLoS One.* 5:e13178.

56. Pache, M., and P. Meyer. 2006. Morphological changes of the retrobulbar optic nerve and its meningeal sheaths in glaucoma. *Ophthalmologica.* 220:393–396.

57. Sigal, I. A., J. G. Flanagan, and C. R. Ethier. 2005. Factors influencing optic nerve head biomechanics. *Invest. Ophthalmol. Vis. Sci.* 46:4189–4199.

58. Song, Z., X. Cao, and H. Huang. 2018. Electroneutral models for dynamic Poisson-Nernst-Planck systems. *Phys. Rev. E.* 97:012411.

59. Fitzhugh, R. 1960. Thresholds and plateaus in the Hodgkin-Huxley nerve equations. *J. Gen. Physiol.* 43:867–896.

60. Gao, J., X. Sun, …, R. T. Mathias. 2000. Isoform-specific function and distribution of Na/K pumps in the frog lens epithelium. *J. Membr. Biol.* 178:89–101.

61. Kofuji, P., and E. A. Newman. 2004. Potassium buffering in the central nervous system. *Neuroscience.* 129:1045–1056.

62. Lauf, P. K., and N. C. Adragna. 2000. K-Cl cotransport: properties and molecular mechanism. *Cell. Physiol. Biochem.* 10:341–354.

63. Falk, G., and P. Fatt. 1964. Linear electrical properties of striated muscle fibres observed with intracellular electrodes. *Proc. R. Soc. Lond. B Biol. Sci.* 160:69–123.

64. Schneider, M. F. 1970. Linear electrical properties of the transverse tubules and surface membrane of skeletal muscle fibers. *J. Gen. Physiol.* 56:640–671.

65. Valdiosera, R., C. Clausen, and R. S. Eisenberg. 1974. Impedance of frog skeletal muscle fibers in various solutions. *J. Gen. Physiol.* 63:460–491.

66. Eisenberg, B., and R. S. Eisenberg. 1968. Selective disruption of the sarcotubular system in frog sartorius muscle. A quantitative study with exogenous peroxidase as a marker. *J. Cell Biol.* 39:451–467.

67. Eisenberg, R. 2015. Electrical structure of biological cells and tissues: impedance spectroscopy, stereology, and singular perturbation theory. *arXiv*, , arXiv:1511.01339 https://arxiv.org/abs/1511.01339.

68. Mathias, R. T., J. L. Rae, and R. S. Eisenberg. 1979. Electrical properties of structural components of the crystalline lens. *Biophys. J.* 25:181–201.

69. Mathias, R. T., J. L. Rae, and R. S. Eisenberg. 1981. The lens as a nonuniform spherical syncytium. *Biophys. J.* 34:61–83.

70. Rae, J. L., R. T. Mathias, and R. S. Eisenberg. 1982. Physiological role of the membranes and extracellular space with the ocular lens. *Exp. Eye Res.* 35:471–489.

71. Hodgkin, A. L. 1937. Evidence for electrical transmission in nerve: Part I. *J. Physiol.* 90:183–210.

72. Hill, A. V. 1932. Chemical Wave Transmission in Nerve. CUP Archive, Cambridge University Press, Cambridge, UK.

73. Villegas, R., and G. M. Villegas. 1960. Characterization of the membranes in the giant nerve fiber of the squid. *J. Gen. Physiol.* 43:73–103.

74. Bracho, H., P. M. Orkand, and R. K. Orkand. 1975. A further study of the fine structure and membrane properties of neuroglia in the optic nerve of Necturus. *J. Neurobiol.* 6:395–410.

75. Pilgrim, C., I. Reisert, and D. Grab. 1982. Volume densities and specific surfaces of neuronal and glial tissue elements in the rat supraoptic nucleus. *J. Comp. Neurol.* 211:427–431.

76. Wang, N. 2019. Intraocular and Intracranial Pressure Gradient in Glaucoma. Springer, Singapore.